9. NECTARIAN SYSTEM

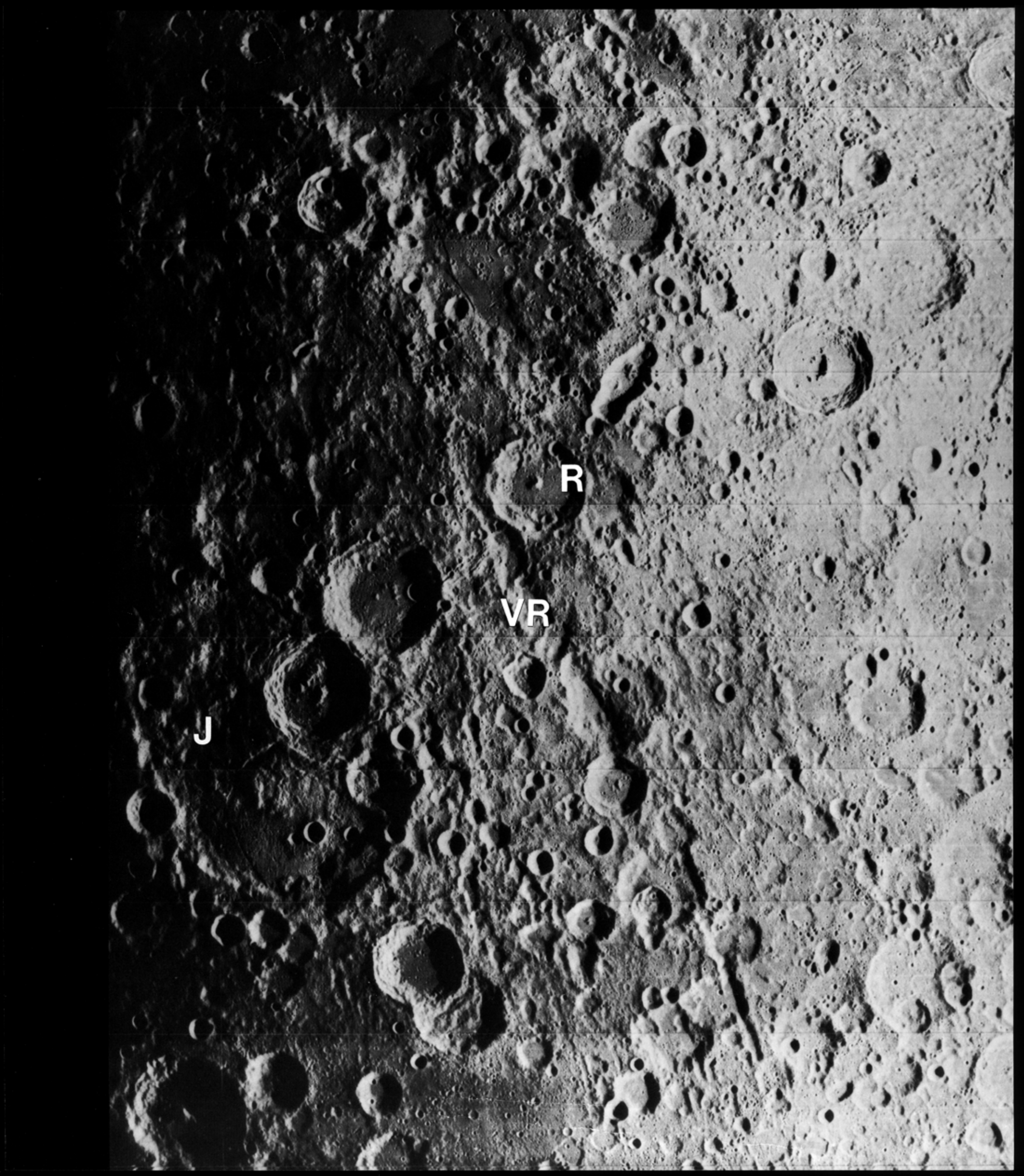

FIGURE 9.1 (OVERLEAF).—Deposits and secondary craters of Nectaris basin southeast of basin rim (upper left). View centered on Vallis Rheita (VR), a Nectaris-basin secondary-crater chain, and crater Rheita, a superposed Nectarian primary-impact crater (R; 70 km, 37° S., 47° E.). Pre-Nectarian terrane is at lower left; largest crater is Janssen (J; 190 km, 45° S., 42° E.). Compare figures 8.15 and 9.2. Orbiter 4 frame M–52.

9. NECTARIAN SYSTEM

CONTENTS

INTRODUCTION

The Nectarian System includes all materials of the Nectaris basin and all younger lunar materials emplaced before the deposition of Imbrium-basin materials (Stuart-Alexander and Wilhelms, 1975). Thus, the Nectarian Period comprises the timespan between the Nectaris and Imbrium impacts. This system contains fewer rock-stratigraphic units than does the pre-Nectarian but is nevertheless widespread on the Moon (pl. 7). Nectarian basin materials cover a large area on the nearside and farside centered on the east limb (figs. 9.1–9.6). Other concentrations are on the farside around the Orientale deposits. Nectarian craters, formed at a declining but still frequent rate (fig. 8.16), are scattered randomly wherever younger deposits are absent or thin. Nectarian plains are more evident than are pre-Nectarian; photogeologic and sample data to be discussed here suggest that some Nectarian plains may be partly volcanic in origin.

Samples were collected from as many as three Nectarian basins. The Apollo 17 mission collected large amounts of material of the Serenitatis basin, which is probably Nectarian. Small fragments returned by Luna 20 from a spot on the Crisium-basin flank probably were emplaced in the ejecta of that Nectarian basin. Apollo 16, arguably, returned materials of the Nectaris basin. As always, the term "Nectarian" in this context refers to the photogeologically observed stratigraphy (see chaps. 2, 7, 8). Most of the materials contained in Nectarian units originated endogenically during the pre-Nectarian, and, additionally, had been extensively reworked by pre-Nectarian impacts before emplacement during the Nectarian Period. In general, the samples can be identified with specific Nectarian stratigraphic units better than with the pre-Nectarian units in which they once resided. The possible Nectaris-basin provenance of the important and controversial Apollo 16 sample suite is discussed in this chapter, and alternative interpretations are weighed in chapter 10.

NECTARIS BASIN

General features

Deposits of the Nectaris basin clearly separate pre-Nectarian and younger Nectarian deposits over a wide area (pls. 3, 7; figs. 8.5, 9.1, 9.2, 9.5, 9.6). At 860 km in diameter, the Nectaris basin is only 70 km smaller than the Orientale basin (table 4.1), and probably resembled Orientale before modification by later basin and crater deposits. The west and south sectors have a moderately well defined ring structure spaced like the Orientale rings (fig. 9.2*A*). In fact, Nectaris was chosen as the type basin by Hartmann and Kuiper (1962).

The landscape south and southeast of the Nectaris basin is a degraded equivalent of the Hevelius Formation and the secondary craters south and southeast of Orientale (figs. 4.4, 9.1; Stuart-Alexander, 1971; Wilhelms and McCauley, 1971; Stuart-Alexander and Tabor, 1972; Stuart-Alexander and Wilhelms, 1975; Wilhelms and El-Baz, 1977). Thick mantling of pre-Nectarian terrane is evident from the paucity of large craters in comparison with the region farther south (figs. 8.5, 9.1). Like the circum-Orientale terrane, the Janssen Formation (fig. 9.2; Stuart-Alexander, 1971) and much other circum-Nectaris terrane are strongly lineate radially to the basin center. Vallis Rheita (figs. 9.1, 9.2) and similar troughs (fig. 9.5; Hodges, 1973b), consist of subtle overlapping or tangential elliptical craters and evidently were formed by secondary impact, as was Vallis Bouvard on the south Orientale-basin flank (fig. 4.4*D*). Subcircular satellitic craters of Nectaris (figs. 9.1, 9.2*B*) also resemble the secondary craters of Orientale in shape, cluster geometry, and distance from the source basin, although they appear less crisp. At Nectaris, the primary-secondary transitional zone that is reproducibly mappable east of Orientale and is also detectable at Imbrium (chap. 4) has been blurred by "aging" and secondary cratering from Imbrium (fig. 3.10*A*); nevertheless, an attempt has been made here to identify the contact

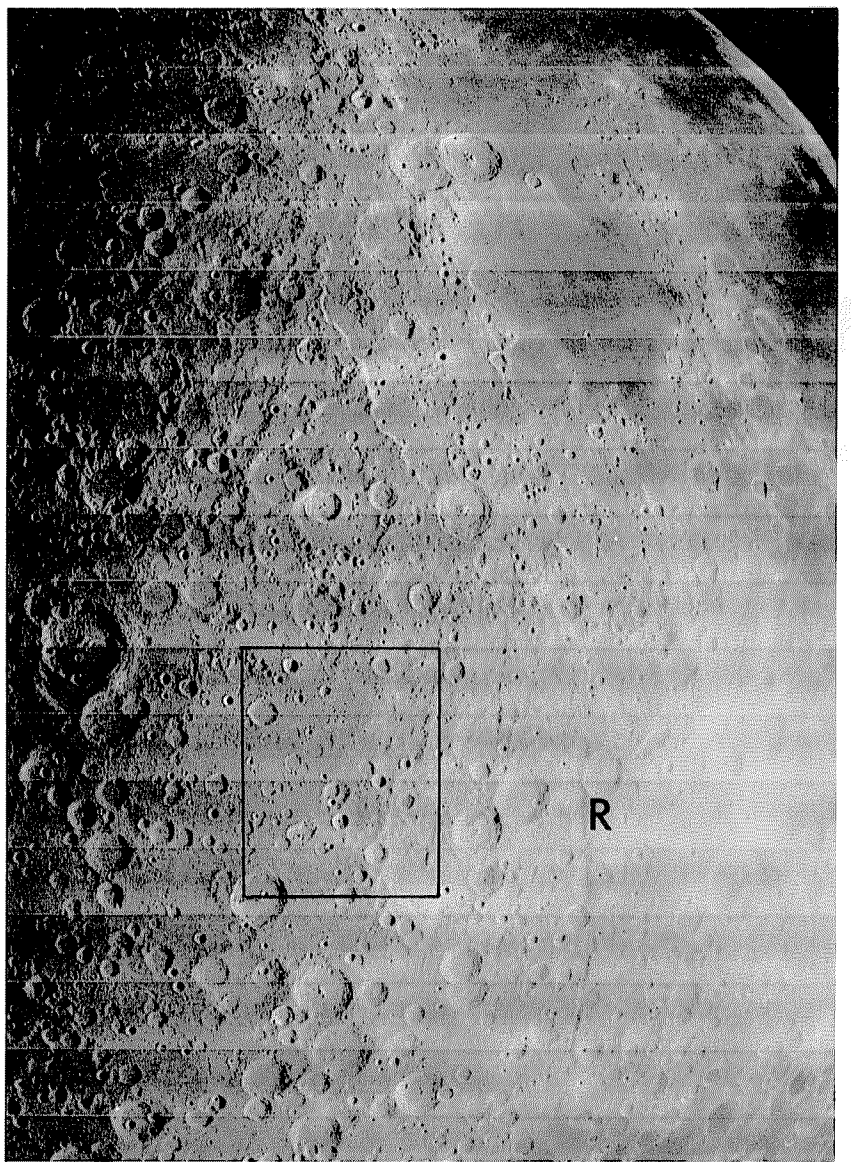

A

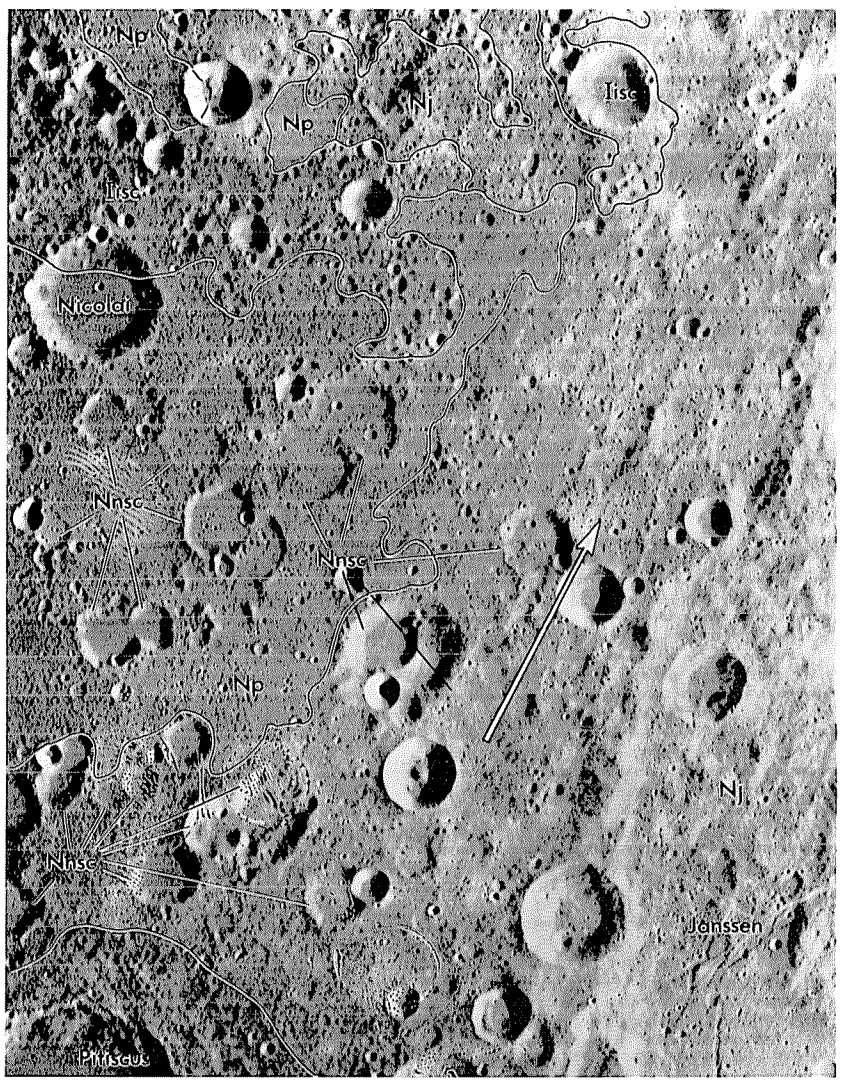

B

between the two Nectaris facies (pls. 3, 7).

The north and east sectors of Nectaris have an overall arcuate map pattern, but individual rings are inconspicuous (fig. 9.7). These sectors resemble western Orientale in this respect (fig. 4.5), although the Nectaris uplifts are more flat-topped than jagged. The northern and eastern Nectaris ejecta is largely buried by younger deposits (pl. 7). Any secondary chains that were formed in these sectors have been buried by younger deposits of the maria and of the post-Nectaris Crisium, Serenitatis, and Imbrium basins (pls. 3, 7; figs. 9.3–9.6).

More light-colored plains are concentrated inside the Nectaris basin than in other settings except the Orientale- and Imbrium-basin peripheries (fig. 10.34). This setting suggests an analogy with the Maunder Formation of Orientale, that basin's interior impact melt. Hummocky material on the northern Nectaris terra is similar in topography and relative position to the Montes Rook Formation and may be the Nectaris equivalent (fig. 9.7; Elston, 1972; Wilhelms, 1972c). However, this hummocky material lies on the distal sides of Imbrium-secondary craters and thus may consist of their decelerated ejecta (Wilhelms, 1980, p. 45).

Light-colored plains are also widespread south of the basin (pl. 7). Wilhelms and McCauley (1971) and Scott (1972b) interpreted the large patches of cratered or "pitted" plains southwest of the basin (fig. 9.2*B*) as volcanic in origin by analogy with the younger, Imbrian plains also thought to be volcanic before the Apollo 16 analyses. The subequal "pits" and larger, also subequal, flat-floored depressions were thought to be volcanic because of their grouping. The superposition of the pitted plains and smoother Imbrian plains on the larger craters was interpreted as analogous to the flooding of craters by mare materials. An alternative explanation, however, seems to be required by the Apollo 16 results. The plains grade with the lineate Janssen Formation, as do circum-Orientale or circum-Imbrium plains with the lineate ejecta of those basins. Therefore, the stratigraphic relations here can be interpreted by the impact model of lunar-terra formation. The large grouped craters are probably Nectaris secondaries, and most of the smaller craters or "pits" are probably Imbrium secondaries. The plains were likely emplaced by one of the ejecta-deposition mechanisms whereby a surge of debris arrives at a site after the secondaries form. This concentration of plains may result from catchment of the Nectaris ejecta by the Mutus-Vlacq basin (fig. 8.12; Wilhelms and others, 1979). In addition, a marelike volcanic deposit, extruded into the Mutus-Vlacq basin during pre-Nectarian time, may underlie the plains and contribute to their level topography (see section below entitled "Volcanic Rocks").

The terrain west of Nectaris differs considerably from that in the other sectors. Rupes Altai (the Altai scarp) constitutes a continuous, well-defined topographic rim (fig. 9.2*A*). Despite its proximity to this rim, the western region contains little evidence of Nectaris ejecta. Thick, strongly lineate ejecta is visible at the same distance from the southwest and southeast rim sectors. Part of the reason for the difference is that the western Nectaris deposits were modified by Imbrium projectiles when the strong Imbrium-radial pattern of craters and grooves was formed (figs. 3.10, 9.2*A*). Additionally, Nectaris ejecta may have been deposited less thickly here than in the south.

Nectaris component in Apollo 16 samples

The thickness of the western Nectaris ejecta is important in the interpretation of samples collected by the Apollo 16 mission. The astronauts landed 60 km west of the Kant Plateau, a broad part of the Nectaris-basin rim crest about 100 km wide (pl. 3; figs. 2.5*C*, 9.8). At Orientale, thick ejecta is visible in the most nearly analogous position, 160 km east of the Cordillera scarp, even though this point is in

FIGURE 9.2.—Materials of Nectaris basin.

A. Regional view showing Mare Nectaris and Nectaris basin (upper right quadrant) and area of *B* (outlined). Letter R is below crater Rheita and right of Vallis Rheita. Orbiter 4 frame M–83.

B. Detail of Janssen Formation (Nj), plains deposits (Np), Nectaris-basin secondary craters (Nnsc), and Imbrium-basin secondary craters (Iisc). Nj, type area of the Janssen Formation (Stuart-Alexander, 1971), which partly buries pre-Nectarian crater Janssen; arrow is radial to center of Nectaris basin. Craters Nicolai (42 km, 42° S., 26° E.) and Pitiscus (82 km, 50° S., 30° E.) are Nectarian. Nj and Np thickly to thinly bury Nnsc; Iisc overlies Nectarian units (Scott, 1972b). Orbiter 4 frame H–83.

the relatively "excluded" zone of ejecta (pl. 3; fig. 4.4*F*). Thus, Nectaris ejecta probably either underlies or composes the surface materials at the Apollo 16 landing site. However, the search for Nectaris materials has been inconclusive.

Two photogeologic units were sampled by Apollo 16. The first is the Cayley Formation, which forms the Cayley plains (figs. 9.8, 9.9). This formation was emplaced during the Imbrian Period (chap. 10); however, it may consist of Nectaris materials reworked during its emplacement. The Cayley was sampled in the central and southern parts of the region (all stations except 11 and 13, fig. 9.9). Station 10, near the landed lunar module (LM) and the geophysical instruments (Apollo Lunar Surface Experiments Package [ALSEP]), is probably the most intensely examined part of the Moon (Muehlberger and others, 1980; Schaber, 1981). Nevertheless, no outcrops or large boulders of the Cayley were found. A regolith 10 to 15 m thick (Cooper and others, 1974; Freeman, 1981) obscures the internal stratigraphy of the Cayley. The Cayley may contain coherent, lithologically uniform strata or lenses (Hodges and Muehlberger, 1981), or may consist of loosely aggregated poorly sorted clastic debris. Some of the mechanisms described in chapter 10 could have emplaced a Cayley Formation consisting of poorly sorted Nectaris debris during the Imbrian Period.

Regolith samples show that impact-melted materials are common in the Cayley Formation (James and Hörz, 1981). Their sources and ages, however, are major problems. A tight compositional cluster (approx 29–31 weight percent Al_2O_3) and a looser cluster (17–21 weight percent Al_2O_3) suggest to Ryder (1981) that two groups of melt rocks came from two distinct melt sheets. The first group is richer in Al than the average terra (25–26 weight percent Al_2O_3; Taylor, 1982) and is mostly subophitic to intergranular in texture, like much volcanic basalt but resulting from thorough impact melting (lithologic type SM, compositional type V, table 9.1). The low-Al samples are the richest in KREEP, are laden with fragmental material, and are typically poikilitic in texture (lithologic type PM, compositional type K). The poikilitic texture results from the relatively mafic composition and from the presence of many clasts, which form nuclei for crystallization of the melt (Lofgren, 1977; Nabelek and others, 1978). In addition, many melt rocks have Al_2O_3 contents intermediate between the two clusters (lithologic type IM, compositional type I); their compositions are commonly described inappropriately as "very high alumina (VHA) basalt" (Hubbard and others, 1973, 1974).

The largest samples of the Cayley Formation were excavated by South Ray Crater, 680 m wide and 130 m deep, which is 2 million years old (table 13.2). Materials probably ejected from South Ray were sampled at stations 4 and 8 (Reed, 1981; Sanchez, 1981; Ulrich and Reed, 1981; Ulrich and others, 1981b). Among other materials is a distinctive dimict (dilithologic) breccia that apparently characterizes the Cayley Formation (James and Hörz, 1981). These "black and white" rocks consist of cataclastic anorthosite and fine-grained impact-melt rock of "VHA" composition. The dimict breccia seems to be analogous to terrestrial dike-breccia deposits formed in the outer parts of impact craters (fig. 3.21). During cratering, melt intruded into cataclastic feldspathic material in the walls of a growing crater or basin and then was quenched, fragmented, and intruded by other clastic feldspathic material (James, 1977, 1981). Fragments of similar anorthosite and melt rock that also abound in the regolith probably originated in dimict breccia.

The melt rocks of the Cayley Formation may have been emplaced while hot as beds or pods (Hodges and Muehlberger, 1981), or they may have been emplaced cold in isolated boulders that South Ray and other craters happened to penetrate. If individual impacts generate uniform melt sheets, one melt type, at most, is likely to have been emplaced hot when the Cayley was emplaced (Ryder, 1981). Thus, reworking of an already complex deposit is suggested. Nonetheless, large single impacts can generate great lithologic and compositional complexities (see chap. 3). It is still unclear how many melt sheets are represented by these melt rocks.

The other unit sampled by Apollo 16 is material of the Descartes Mountains (fig. 9.9; Milton and Hodges, 1972). For convenience, this unit is here called the Descartes Formation, although it has not been defined formally. The Descartes is divided into two gradational facies. The northern or Smoky Mountain facies is grooved radially to the Imbrium basin. Grooves in the southern or Stone Mountain facies curve away from this Imbrium-radial direction into a more nearly transverse trend approximately where the formation contacts the Kant Plateau (figs. 2.5*C*, 9.9). This embankment of the Descartes Formation against the Nectaris-basin rim has been considered as evidence for a partial Nectaris origin of the topography (Head, 1972; Wilhelms, 1972c). Thus, both the Imbrium and Nectaris basins may have contributed to the morphology of the Descartes Formation; the same is true for the materials of which it is composed.

Large sample collections were made at stations 11 and 13 on Smoky Mountain from ejecta of the 1-km-wide, 50-million-year-old (table 13.2) North Ray Crater (fig. 9.10; Stöffler and others, 1981; Ulrich and others, 1981b). Station 11 is on the crater rim, and station 13 is about one crater diameter from the rim (fig. 9.9). North Ray penetrated a 50-m-high mass-wasted ridge that is part of Smoky Mountain (300–400 m high overall). The 230-m depth of North Ray probably ensures that the Smoky Mountain material was excavated (Ulrich, 1973; Ulrich and others, 1981b). The station 11 and 13 samples are mostly of fragmental feldspathic breccia whose fragmental melt-poor matrix is composed of material similar to that of the larger clasts (fig. 9.10). About half the clasts are of cataclastic anorthosite (Minkin and others, 1977; James, 1981), a quarter of granulitic breccia, and a quarter of feldspathic fragment-laden impact melt (lithologic types CA, G, and FM, respectively, table 9.1). The granulitic breccia is thermally metamorphosed (Warner and others, 1977; James, 1980, 1981). The relation of the FM-type melts to the breccia deposit in which they are found is not known. They may have been cogenetic with the fragmental breccia (as in suevite at the Ries; see chap. 3; Stöffler and others, 1979) or may predate the deposition of the breccia. Determining which is the case here would be an important step in interpretation of the Descartes Formation, especially considering the rarity of impact melts in the breccia matrices; such melts are generally the most valuable for dating impact deposits.

Small amounts of the Stone Mountain facies may have been sampled at stations 4 and 5, where feldspathic material like that at stations 11 and 13 was recovered. Contamination by Cayley material

---

Note: Figures 9.3 through 9.6 constitute a series of overlapping oblique photographs taken by Lunar Orbiter 4 of areas covered poorly from lower altitudes earlier in the mission (pl. 2); Sun illumination is opposite from that in other nearside photographs.

FIGURE 9.3. (p. 166, left)—Part of northeast quadrant of nearside, including Mare Crisium and Crisium basin (bottom; centered at 17.5° N., 58.5° E.). Major Nectarian craters are Cleomedes (Cl; 126 km) and Endymion (E; 125 km; pl. 7; table 9.4). Arrows indicate secondary-crater chains radial to Crisium (C) and Imbrium (I) basins; terra south of dashed line is covered by deposits of Crisium basin, except where covered by younger deposits of Cleomedes, Geminus (G; 86 km, Eratosthenian), and Taruntius (T; 56 km, Copernican). A, Atlas (87 km, Lower Imbrian); H, Hercules (69 km, Eratosthenian); M, Messala (124 km, pre-Nectarian, partly covered by Crisium deposits). Orbiter 4 frame H–191.

FIGURE 9.4. (p. 166, right)—Part of northeast quadrant near east limb, including two distinct rings of Humboldtianum basin (300- and 600-km diameter, centered at 61° N., 84° E.) between Mare Humboldtianum (H) and crater Endymion (E; compare fig. 9.3). Arrows indicate Humboldtianum-radial or -subradial directions; arrow I is also radial to Imbrium (fig. 9.3), and arrow below crater Zeno (Z) is also radial to Crisium. Zeno is superposed on Humboldtianum basin and overlain by Crisium-basin secondary-crater cluster (compare fig. 4.3*Q*). Deposits and clustered craters between Gauss (G; 177 km, a Nectarian crater with fractured floor) and Joliot (J; 143 km, pre-Nectarian) are probably outer materials of Humboldtianum basin; deposits in lower third of photograph may be related to Crisium (C). Basin deposits underlie Nectarian craters Gauss, Berosus (B; 74 km), and Neper (N; 137 km, 9 N., 85 E.), Lower Imbrian crater Hahn (Ha; 84 km), and mare basalt (M; Mare Marginis) (compare fig. 4.7). Orbiter 4 frame H–165.

FIGURE 9.5. (p. 167, left)—Terrain south of Mare Crisium (C) and east of Nectaris basin. Black-and-white arrows are radial to basin centers and denote large secondary-crater chains of Crisium basin (c) and Nectaris basin (N; lower chain is part of Vallis Rheita); g, graben. Outer deposits of Crisium (Nco) and Nectaris (Nno) include secondary craters and terra-mantling deposits. Luna 20 landing site (L20) is on Crisium-basin rim (compare fig. 11.16). Nj, Janssen Formation, partly covers pre-Nectarian crater Furnerius (F; 125 km, 36° S., 60° E.). Np, plains of Nectarian age; INp, deposit in pre-Nectarian Balmer-Kapteyn basin, probably consisting of Nectarian plains overlain by Imbrian plains. y, deposits younger than Nectarian. Primary and secondary deposits of floor-fractured Lower Imbrian crater Petavius (P; 177 km) are superposed on plains, Crisium-secondary chain (c; Vallis Palitzsch), and crater Adams (A; 66 km); Adams and Pontecoulant (Po; 91 km, 59° S., 66° E.), both Nectarian, overlie basin deposits. L, Langrenus (132 km), an Eratosthenian crater superposed on Crisium deposits and Mare Fecunditatis. Orbiter 4 frame H–184.

FIGURE 9.6. (p. 167, right)—Eastward continuation of geology shown in figure 9.5. Southward extent of Crisium-basin deposits (Nco) is obscured by large, floor-fractured, Upper Imbrian crater Humboldt (H; 207 km, 27° S., 81° E., unrelated to Humboldtianum basin); clustered craters between H and arrow N (indicating Nectaris center) may be Crisium-basin secondaries. C, direction to center of Crisium; Nno, outer deposits of Nectaris basin. Po, Pontecoulant (91 km, 59° S., 66° E.); m, part of Mare Australe. Orbiter 4 frame H–178.

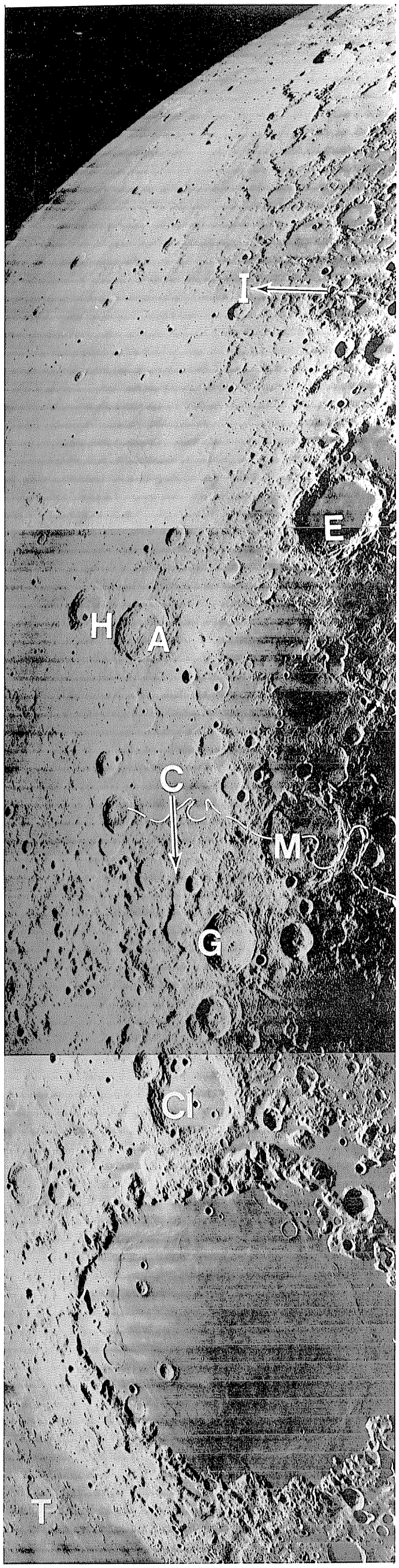
I
E
H
A
C
M
G
Cl
T

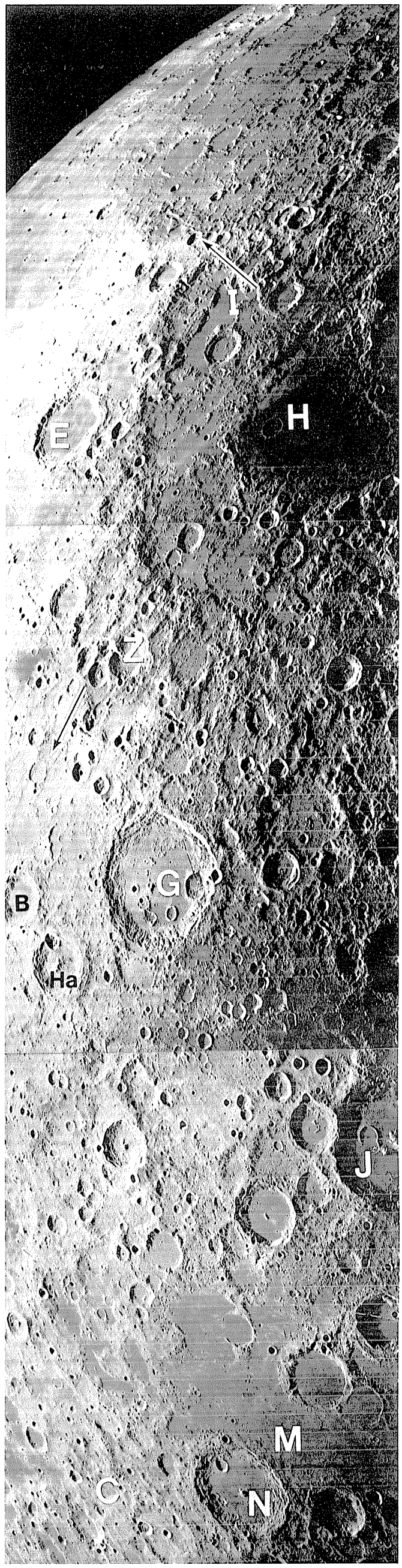
I
H
E
Z
G
B
Ha
J
M
C
N

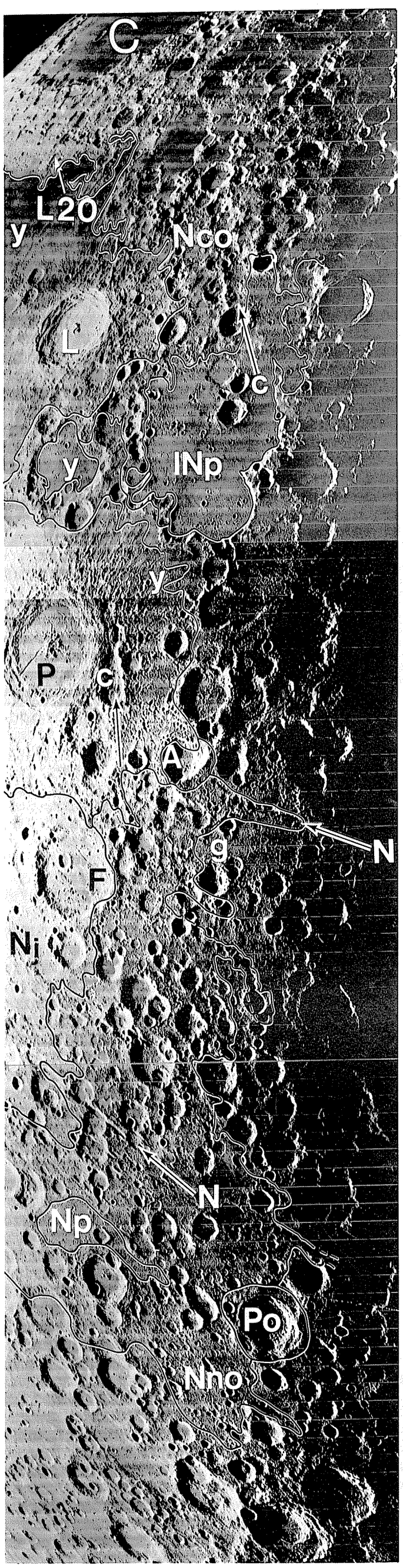
C
L20
y
Nco
L
c
y
INp
y
P
c
A
g
N
F
Ni
N
Np
Po
Nno

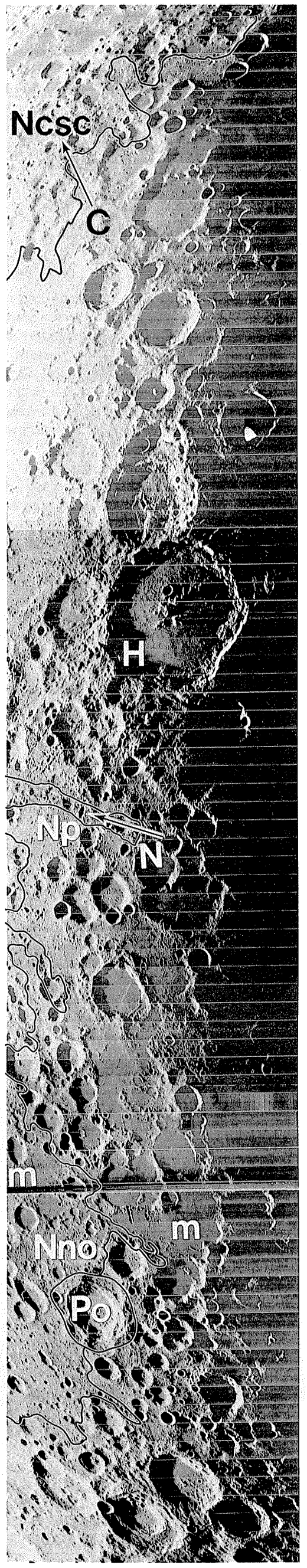
Ncsc
C
H
Np
N
m
m
Nno
Po

(or a similarity of Cayley and Descartes material), however, is likely at those stations, considering that many large samples consist of dimict breccia with a 2-million-year exposure age (Sanchez, 1981).

In summary, the Cayley and Descartes Formations appear to differ in several respects in addition to morphology (James, 1981; James and Hörz, 1981; Stöffler and others, 1981). (1) The North Ray Crater samples (probable Descartes) are more aluminous than the South Ray Crater samples (Cayley). (2) The Cayley appears to contain more impact-melt rock, whereas the Descartes is characterized by friable fragmental feldspathic breccia. (3) More of the Cayley impact-melt rocks are of low-K KREEP and "VHA" composition. (4) The Cayley apparently has a higher magnetism as measured on the surface, a possible indication of buried melt-rich breccia (Strangway and others, 1973). Finally, (5), the Cayley is characterized by sharper craters, more blocks ejected onto the surface from craters, and a thinner regolith (Ulrich, 1973), properties consistent with the Cayley being a more cohesive unit than the Descartes. A possible explanation for these lithologic and topographic differences is that the Descartes Formation consists mostly of Nectaris ejecta and the Cayley of melt-rich Imbrium ejecta.

This complex region is still not well understood. Neither the Cayley nor the Descartes Formation can be said to be well characterized lithologically or stratigraphically. Apart from a boulder composed of lithified regolith (sample 62195), the only boulders sampled are those from North and South Ray Craters. The observed differences may not be qualitative but may reflect relative proportions of the same constituents (O.B. James and M.M. Lindstrom, oral commun., 1983). Analyses of the returned samples have stressed their highly feldspathic composition, and only now are beginning to address problems of the origin and emplacement age of the breccia deposits.

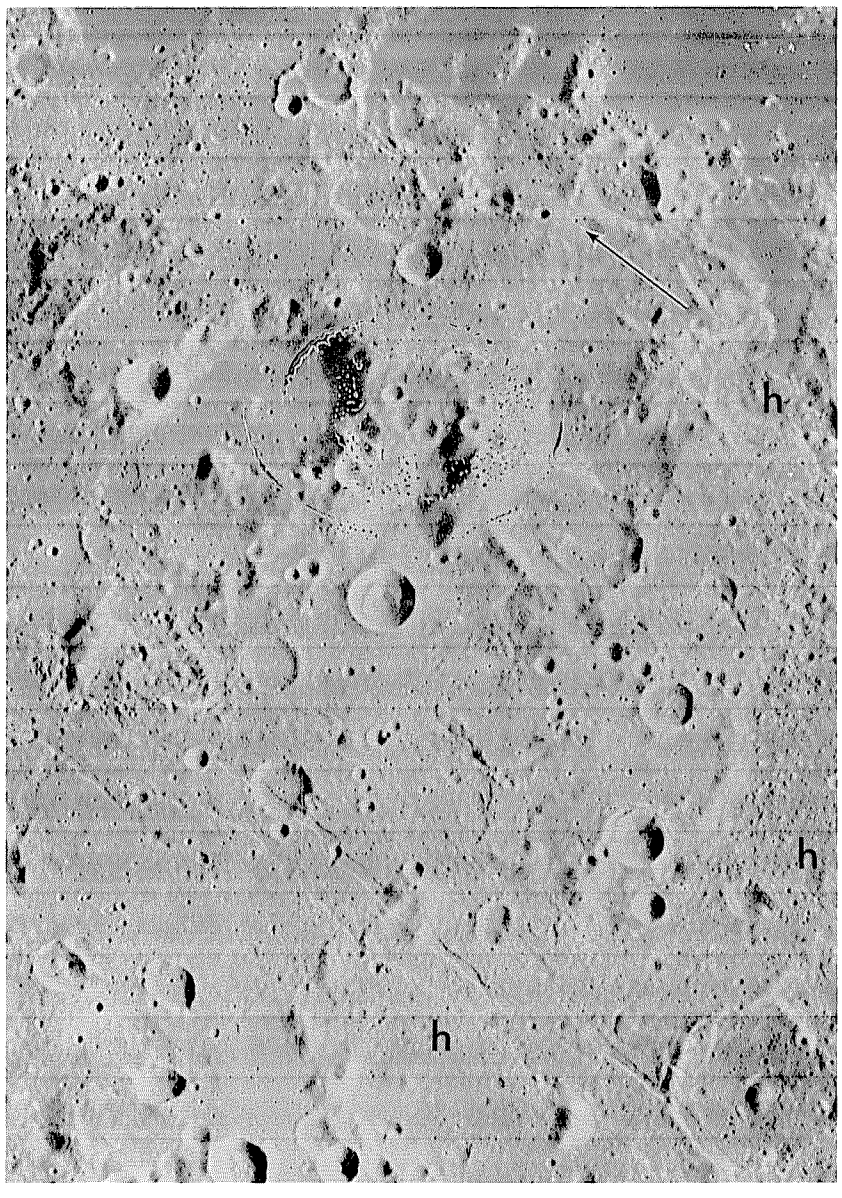

FIGURE 9.7.—North rim of Nectaris basin. Hilly terrain (h) is possible Nectaris equivalent of Montes Rook and Alpes Formations. Topographic freshness, however, suggests emplacement by Imbrium-basin secondary craters (arrow is radial to Imbrium). Imbrium-radial grabens are in lower third of photograph (see chap. 6). View centered at 3° S., 37.5° E. Orbiter 4 frame H–72.

TABLE 9.1.—*^{40}Ar-^{39}Ar ages of Apollo 16 samples*

[After James (1981).
Sample numbers (Ulrich and others, 1981): 60-, station 10, central part of area near Lunar Module and Apollo Lunar Science Experiment Package (ALSEP); 61-, station 1, central area on rim of 300-m-diameter Flag Crater; 615-, chips from rake sample 61500; 63-, station 13, on ejecta of North Ray Crater, about 800 m from rim: 635-, 2- to 4-mm fines from rake sample 63500; 64-, station 4, on Stone Mountain; 65-, station 5, on Stone Mountain; 66-, station 6, near base of Stone Mountain; 67-, station 11, on southeast rim of North Ray Crater; 676-, 2- to 4-mm fines from rake sample 67600; 677-, 2- to 4-mm fines from rake sample 67700; 68-, station 8, on ejecta of South Ray Crater, 3.3 km northeast of rim; 685-, fragment from rake sample 68500; identical to DM (see below). Digits and letters after commas refer to splits of sample.
Lithologies: CA, cataclastic (mechanically disrupted) anorthosite, found as clasts in feldspathic fragmental breccia, as one of the major lithologies in dimict breccia, and as monolithologic fragments in the regolith; some recrystallized. DC, anorthosite in dimict breccia. DM, impact-melt rock in dimict breccia; texturally diverse; mostly fine grained, compositionally uniform melt-rock component of the breccia. FM, feldspathic fragment-laden impact-melt rock; diverse texture, nonpoikilitic. G, granulitic breccia (granulitic impactite of Warner and others, 1977); probably recrystallized or partially melted after heating of earlier breccia (Warner and others, 1977; James, 1980, 1981); compositionally heterogeneous: granulitic (granoblastic) texture consists of small equant crystals lacking well-developed crystalline forms. IM, intergranular impact-melt rock; fine texture: intergranular texture consists of pyroxene filling voids between plagioclase crystals. PM, poikilitic impact-melt rock: poikilitic texture consists of large single grains (commonly of pyroxene) enclosing many small crystals (commonly of plagioclase). SM, subophitic impact-melt rock; fine texture, grading to intergranular; glassy residuum also present: subophitic texture consists of pyroxene filling voids and partly surrounding plagioclase crystals.
Al_2O_3 contents from Ryder and Norman (1980) and James (1981).
Surface unit is unit in which sample was emplaced at surface and from which it was collected (Ulrich and others, 1981): Ca, Cinco a crater: local, in regolith developed from underlying unit; NR, rim or other ejecta of North Ray Crater; SR, ejecta of South Ray Crater.
Source unit is photogeologic unit in which sample was emplaced near the landing site: C, Cayley Formation; D, Descartes Formation.
Ages recalculated from original values, using International Union of Geological Sciences (IUGS) decay constants (Steiger and Jäger, 1977), except for those determined by Schaeffer and Husain (1973, 1974), Schaeffer and others (1976), and Schaeffer and Schaeffer (1977); reevaluation of the monitor used by these analysts nearly compensates for the changes in decay constants (O. A. Schaeffer, in James, 1981, p. 210).
References: H73, Huneke and others (1973); J74, Jessberger and others (1974); J77a, Jessberger and others (1977a); K73b, Kirsten and others (1973b); M78, Maurer and others (1978); P75, Phinney and others (1975); S73, Stettler and others (1973); S76, Schaeffer and others (1976); SH73, Schaeffer and Hussain (1973); SH74, Schaeffer and Husain (1974); SS77, Schaeffer and Schaeffer (1977); T73, Turner and others (1973); TC75, Turner and Cadogan (1975)]

Sample	Lithology	Al_2O_3 (wt pct)	Surface unit	Source unit	Age (aeons)	References
60015,22	CA	35±	SR	C	3.50±0.05	SH74, P75.
68415,49	SM	25-30	SR or local	C	3.74±0.04	S73.
68415,10	SM	27	SR or local	C	3.80±0.04	H73.
68415,50	SM	25-30	SR or local	C	3.80±0.06	K73b.
67603,1-ME	PM	27	NR	D	3.83±0.05	M78.
65015,61	PM?	20±	?	?	3.86±0.04	K73b.
63503,17-LN	IM	23	NR	D	3.87±0.04	M78.
65055,12B	SM	?	SR?	C?	3.89±0.02	J77a.
67703,14-NF	G	29	NR	D	3.89±0.04	M78.
67703,14-NG	G	28	NR	D	3.89±0.04	M78.
67016,100	?	30±	NR	D	3.89±0.05	TC75.
67603,1-MQ	G	28	NR	D	3.90±0.06	M78.
65055,12A	SM	?	SR?	C?	3.90±0.02	J77a.
64536,3	DC	?	SR or Ca	C	3.91±0.01	J77a.
60315,6,1	PM	17±	SR or local	C	3.91±0.02	S76.
67703,14-NI	PM	25	NR	D	3.91±0.04	M78.
67703,14-ND	SM	24	NR	D	3.91±0.04	M78.
64535,7	DC	?	SR or Ca	C	3.92±0.02	J77a.
65015	PM	20±	?	?	3.92	J74.
63503,17-LE	G	33	NR	D	3.92±0.04	M78.
63503,17-LC	G	25	NR	D	3.93±0.04	M78.
68416,34	SM	25-30	SR	C	3.94±0.05	K73b.
63503,17-LK	IM	26	NR	D	3.94±0.05	M78.
68503,16,33	IM	23	Local	C	3.95±0.06	SH73.
63503,17-LI	G	31	NR	D	3.96±0.04	M78.
67603,1-MD	FM	32	NR	D	3.96±0.05	M78.
60315,19	PM	<20	SR or local	C	3.97±0.03	K73b.
65785,13	SM	20-25	Local	D	3.97±0.02	SS77.
67075	CA?	>30	NR	D	3.98±0.05	T73.
68503,16,1	PM	?	Local	C	4.00±0.05	SH73.
66043,2,5	PM	?	Local	D?	4.01±0.05	SH73.
61503,1,11	PM	?	?	?	4.02±0.02	SS77.
61503,1,18	IM	23	?	?	4.02±0.01	S76.
68415,10	Plagioclase	25-30	SR?	C	4.03±0.04	H73.
63503,17-LH	FM	33	NR	D	4.09±0.07	M78.
67603,1-MM	FM	31	NR	D	4.10±0.05	M78.
67703,14-NL	FM	32	NR	D	4.12±0.05	M78.
63503,17-LL	FM	33	NR	D	4.13±0.04	M78.
63503,17-LF	FM	33	NR	D	4.13±0.1	M78.
67703,14-NN	FM	32	NR	D	4.14±0.04	M78.
60025,86	DC?	35±	SR	C	4.17-4.21	SH74.

Absolute age

Absolute ages determined by the ^{40}Ar-^{39}Ar method on materials obtained from the Cayley and Descartes Formations do not clearly indicate a difference in provenance consistent with the suggested lithologic differences. Pre-Imbrian ages (older than 3.85 aeons) are more common than Imbrium-basin ages. The following interpretation suggests an age for the Nectaris basin (James, 1981).

The dated material that is most critical with respect to a Nectaris-basin age was derived from the feldspathic fragmental breccia deposits penetrated by North Ray Crater (table 9.1). Coarse fines (2–4 mm) of melt type FM collected by rake from the North Ray regolith yielded a cluster of six dates between 4.09 and 4.14 aeons and one younger date of 3.96 aeons (Maurer and others, 1978). Because the young fragment (67603,1–MD) is compositionally and texturally identical to the apparently older clasts, 3.96 aeons is a maximum age for the FM-type materials (James, 1981). The older ages were probably inherited from an earlier event and were not reset when the feldspathic fragmental breccia deposits were assembled. Their close clustering suggests an actual event at about 4.1 aeons. Wetherill (1981) suggested that the older event was the Nectaris impact, whereas Maurer and others (1978) and James (1981) proposed that it was a pre-Nectarian crater impact(s).

The other chronologically significant type of coarse fines derived from the feldspathic fragmental breccia deposits is granulitic breccia. The ages of six fragments range from 3.89 to 3.96 aeons, a range that also includes the age of the youngest FM-type melt (Maurer and others, 1978). This range may reflect analytical inaccuracies and may record a single metamorphic episode generated by a major source of near-surface heat, probably a hot basin-ejecta blanket (Warner and others, 1977). The geologic setting of the samples suggests the Nectaris ejecta as the source of this heat. The average of the age cluster, 3.92 aeons, or the youngest age, 3.89 aeons, which is also the age of a dark clast and a plagioclase separate from sample 67016 (Turner and Cadogan, 1975), may date the Nectaris impact (Jessberger and others, 1974; Turner, 1977; Maurer and others, 1978; James, 1981).

The wide range of isotopic ages presents obvious problems for determining the emplacement ages of the Cayley and Descartes Formations. An age occupies almost every 10-million-year interval from 4.14 to 3.86 aeons ago, and four ages are younger (table 9.1). The inevitably long list of uncertainties includes: (1) analytical errors; (2) incomplete reequilibration of argon isotopes by impacts; (3) addition or removal of argon by later events; (4) varying degrees of equilibration of clasts and matrices in the same sample, which are commonly analyzed together; (5) failure to collect thoroughly reset materials that do date an event; (6) uncertainty whether the recorded events are the crystallization of plutonic rocks, metamorphism (granulitic breccia), the main emplacing impact, or minor later impacts; and (7) uncertainty whether the photogeologic unit underlying the sampling stations was actually sampled (especially questionable for the

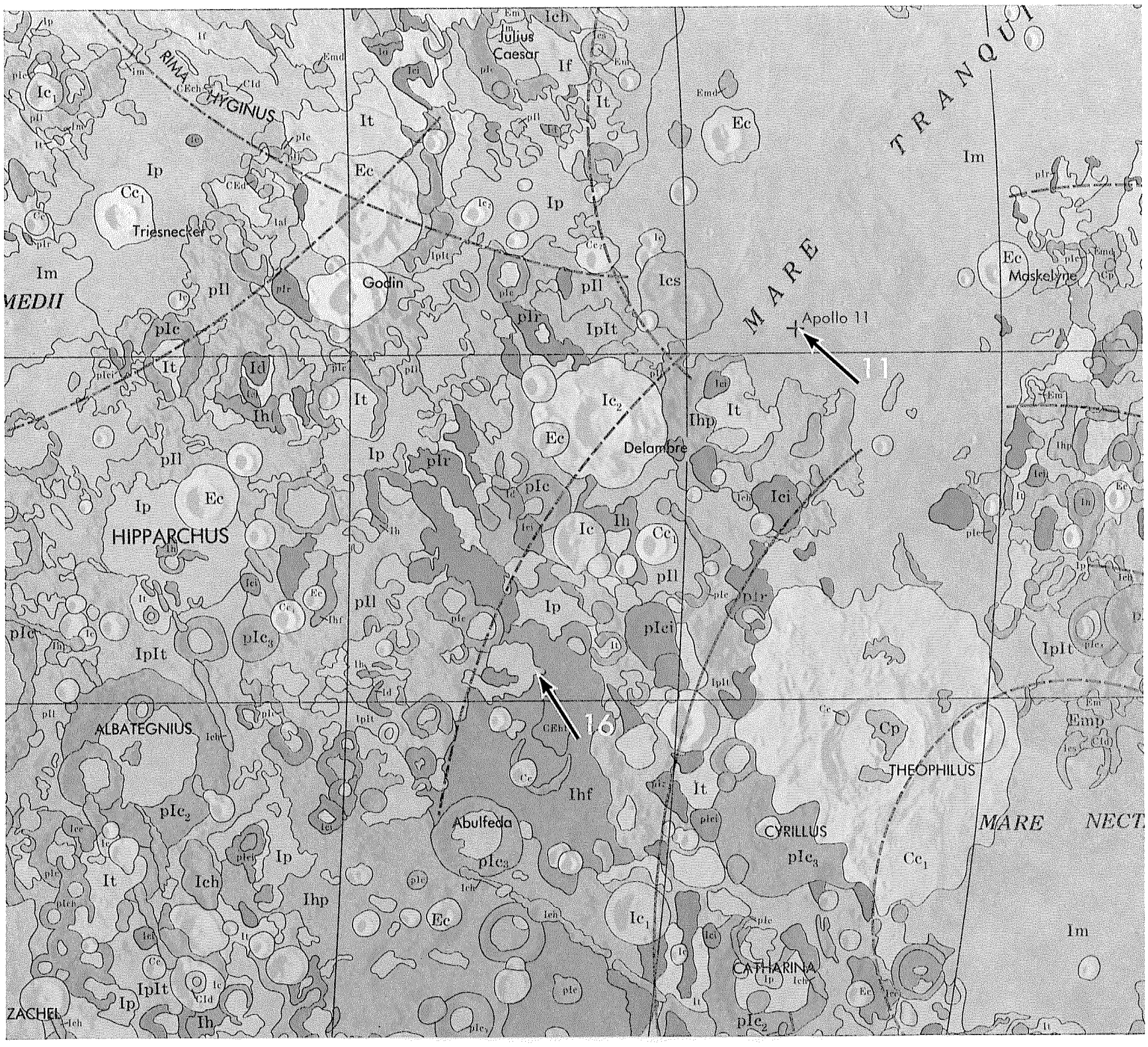

FIGURE 9.8.—Geologic map of part of nearside (Wilhelms and McCauley, 1971), including Apollo 11 (see chap. 11) and Apollo 16 landing sites. Im, mare basalt of Imbrian age (Apollo 11); Ip, plains material of Imbrian age (Cayley Formation; Apollo 16); Ihf, hilly and furrowed material of Imbrian age (Descartes Formation; Apollo 16). Arcs indicate basin rings as interpreted at time of map's preparation.

Descartes Formation). The problems are illustrated by sample 60315 from the Cayley, which yielded ages of 3.91 to 3.97 aeons (table 9.1). Therefore, the dating may not be accurate; the ages listed in table 9.1 may date no real event at all.

These ages, however, are at least consistent with formation of the Nectaris basin at about 3.92 ± 0.03 aeons, and this date is tentatively accepted in this volume (fig. 8.16). The basin is unlikely to be younger than that age range because no samples of granulitic breccia or type-FM melt rock recovered from the Descartes Formation have yielded younger ages (James, 1981). It is unlikely to be older than that age range because some type-FM melts were reset during that time interval, because metamorphism of granulitic breccia requires a major heat source not available after the Nectaris impact, and because the impact-rate curve (fig. 8.16) would have to bend to fit both the available Imbrian ages and an older age for Nectaris (see chap. 8). The ages older than 3.92 ± 0.03 aeons (table 9.1) date pre-Nectarian events, if they date any discrete events. The few younger ages may have been introduced or partly reset during the Imbrium impact by the mechanisms described in chapter 10.

CRISIUM BASIN

General features

Crisium has already been referred to in connection with basin topography, ring origin, mare-basalt thickness, and structural modification because quantitative data were obtained by overflights of

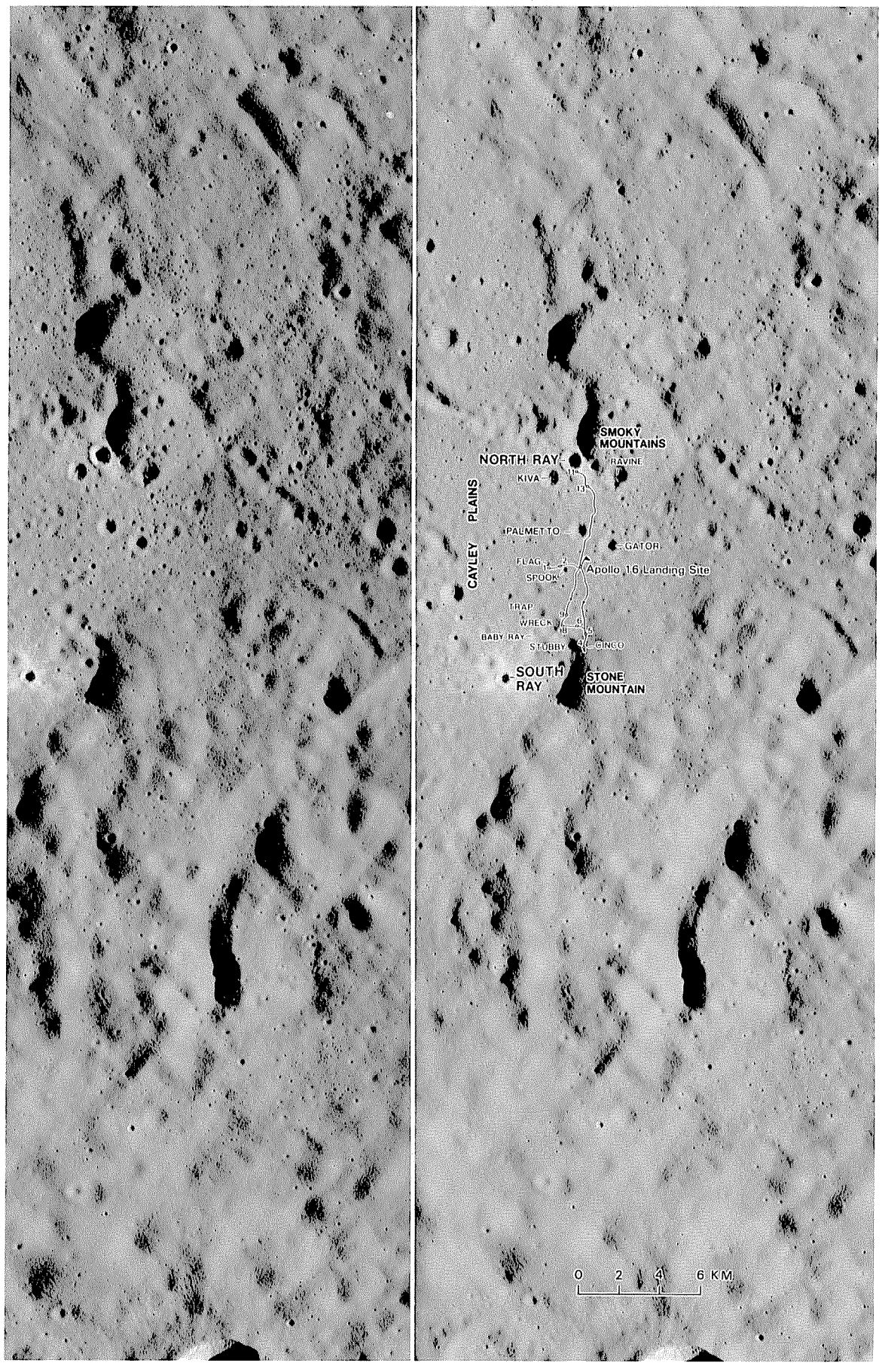

FIGURE 9.9.—Region of Apollo landing 16 site. Facies of the Descartes Formation in the Smoky Mountains is furrowed radially to Imbrium basin; facies in Stone Mountain is furrowed transversely to Imbrium and radially to Nectaris basin. Lines, astronaut traverses; numbered circles, sampling stations. Stereoscopic pair of Apollo 16 frames P–4558 (right) and P–4563 (left).

Apollo 15 and 17 instruments (pl. 2; figs. 4.9, 5.23). As in many large basins, the identity of its topographic rim is unclear. The massive mare-bounding rim, about 635 km in diameter, would seem to be the logical choice as the topographic rim and, therefore, the boundary of excavation. It probably does bound a deep cavity. Incomplete but locally conspicuous arcs, however, form a near-circle, 1,060 km in diameter, whose massifs are as high as or higher than those of the 635-km-diameter ring (figs. 4.3*Z*, 4.9, 9.11). These arcs are locally rimlike (raised crest, steep inner slope, gentler outer flank) and mark the inner boundary of conspicuous secondary chains (figs. 9.3, 9.5, 9.6). Thus, the outer zone may have been partly excavated. A large basin excavation is consistent with the many topographic complexities within the 1,060-km periphery, and that diameter is favored here as the excavation diameter of Crisium.

Another fact favoring a large excavation is the probable great extent of the ejecta and secondary craters. Crisium-secondary craters extend as far as 900 km northward and 1,100 km southward of the basin center (pl. 7; figs. 9.3–9.6). One group of secondaries seems to be superposed on the crater Zeno, which, in turn, is superposed on the Humboldtianum basin (fig. 9.4). The extent of the continuous ejecta is less clear. Hummocky terrain occupies some sectors close to the basin, as does the somewhat similar, though topographically sharper, Montes Rook Formation of Orientale (fig. 9.11; Scott and Pohn, 1972; Scott and others, 1972; Head, 1974b; Wilhelms, 1973, 1980). Crisium ejecta probably covers terrain in the poorly photographed zone east of Crisium, which is smoother than the adjacent more heavily cratered pre-Nectarian terrane (fig. 9.4). An extent of Crisium ejecta as great as 1,600 km east of the Crisium center is suggested by a concentration of radially arranged craters 10 to 20 km in diameter.

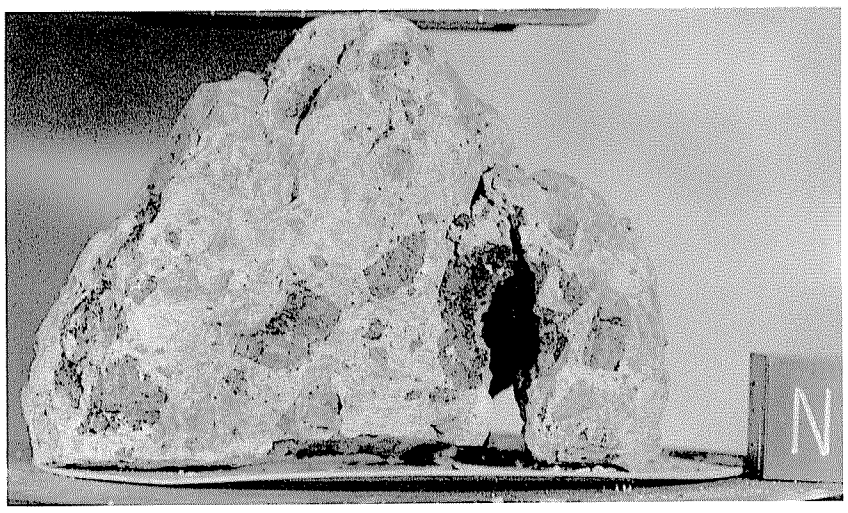

A

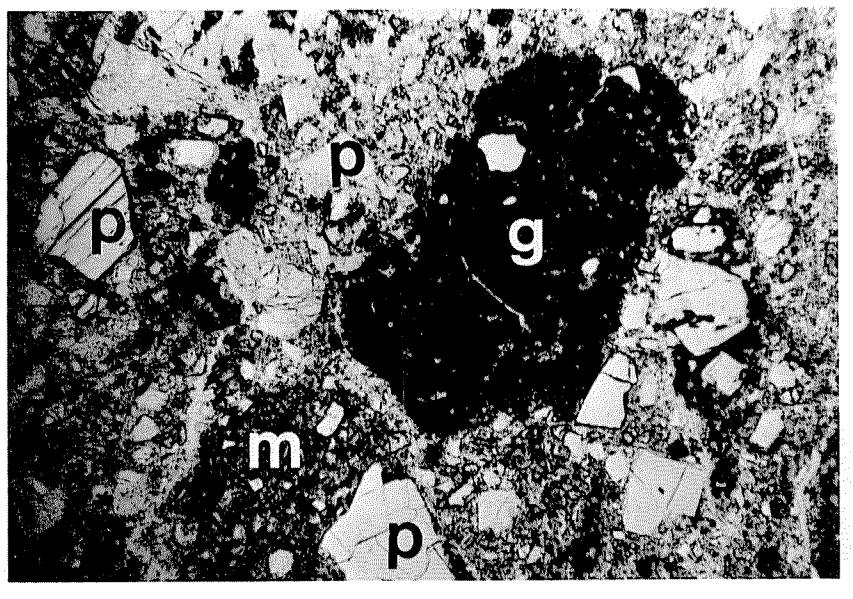

B

FIGURE 9.10.—Feldspathic fragmental breccia (sample 67015) collected from rim of North Ray Crater.

A. Whole sample. Melt-rich clasts are dark; light material includes feldspathic matrix and clasts. Sides of cube (letter N), 1 cm. Courtesy of Lunar and Planetary Institute, Houston, Tex.

B. Thin section of sample 67015,88. Seriate-textured matrix consists of cataclastic plagioclase and minor pyroxene. Clasts include glassy-matrix breccia (g), clast-laden, crystalline impact-melt breccia (m), and monomineralic plagioclase (p). Plane-polarized light; field of view, 1.5 mm. Courtesy of P.D. Spudis.

The observed pattern of Crisium ejecta is three-pronged, rather like that of the crater Messier (fig. 3.11*A*). A further similarity with Messier is the elliptical outline of Crisium, elongate approximately east-west. The east sector of the mare-bounding ring is almost missing (fig. 4.3*Z*). An oblique impact from the west, possibly by a fragmented body, is suggested as the cause of these asymmetries (table 4.4).

Luna 20 samples

The Luna 20 mission returned a small core of regolith material from a part of the Crisium flank that is outside the mare-bounding rings and that is here considered to lie inside a buried part of the main rim (pls. 3, 7; fig. 9.5). Most of the fragments are of aluminous ANT rock not unlike the Apollo 16 suite; some are of low-K KREEP composition (Prinz and others, 1973; Taylor, G.J., and others, 1973). They have been dated at 3.84 ± 0.04 aeons (Podosek and others, 1973), an age consistent either with a late Nectarian relative age of Crisium or with an Imbrian age of superposed Imbrium-basin or Imbrian-crater material. In view of the small size of the sample and the difficulties encountered in dating the larger Apollo 16 and 17 sample suites, no firm conclusions should be based on this age despite its apparent analytical precision.

SERENITATIS BASIN

General features

Although Mare Serenitatis is one of the Moon's most conspicuous circular maria (fig. 1.7), the Serenitatis basin is indistinct and was not even listed as a basin by Hartmann and Kuiper (1962). Its west sector has been nearly destroyed by the Imbrium basin, and its north rim is covered by hummocky Imbrium ejecta (Alpes Formation; figs. 1.7, 10.12). The map pattern of the north rim and the presence of two mascons suggest that Serenitatis consists of a smaller northern basin and a larger southern basin (Baldwin, 1963, p. 320; Scott, 1972a, 1974; Reed and Wolfe, 1975; Wolfe and Reed, 1976; Head, 1979c). Although two independent impacts have been proposed, the considerable evidence for multiple simultaneous crater impacts (see chap. 3) and basin impacts (Humboldtianum, Moscoviense, possibly Crisium) suggests such an origin here as well. Montes Haemus, the south topographic rim of Serenitatis or "South Serenitatis," is conspicuous, though covered by lineate and smooth Imbrium ejecta (figs. 1.7, 9.12).

The east sector is of most interest because part of it was sampled by Apollo 17. The terra east of Mare Serenitatis consists of angular massifs that are partly concentric and partly radial to the mare (fig. 9.13). A general ring form is visible, but no single ring stands out. The largest massifs surround the Taurus-Littrow valley, in which Apollo 17 landed. The vague ring containing these massifs resembles the outer Rook ring of Orientale (Head, 1974b, 1979c; Reed and Wolfe, 1975; Solomon and Head, 1979). Although parts of an indistinct ring east of the Littrow massifs and ending near the crater Vitrivius (fig. 9.3) are higher than the massifs (Head, 1979c), this "Vitruvius front" is not sharply delineated like Montes Cordillera of Orientale. Therefore, eastern Serenitatis resembles the irregularly structured western Orientale more closely than it does the regularly ringed eastern Orientale (fig. 4.1). As is common for large basins, the east boundary of the excavation cavity of Serenitatis is thus poorly defined.

One possibility is that the Vitruvius front is the excavation boundary; small amounts of material may have been ejected from the zone between the Littrow and Vitruvius rings, as proposed above for Crisium and in chapter 4 for other large basins. The most straightforward interpretation, however, is that the excavation boundary passes along the east edge of Mare Serenitatis through the largest massifs of the Littrow ring (figs. 5.17, 9.12, 9.13). I tentatively favor this interpretation despite the similarity of the Littrow ring to the outer Rook ring, which I believe lies inside the basin excavation. A diameter of about 740 km—190 km smaller than Orientale—fits the largest Littrow and Haemus massifs. This identification of the rim is strengthened by Whitaker's (1981) interpretation of the Vitruvius ring as a part of the middle ring of the Procellarum basin (pl. 3; fig. 9.11)—an interpretation that also explains why the terra east of Serenitatis is so irregular and why no relation of rings to basins is obvious.

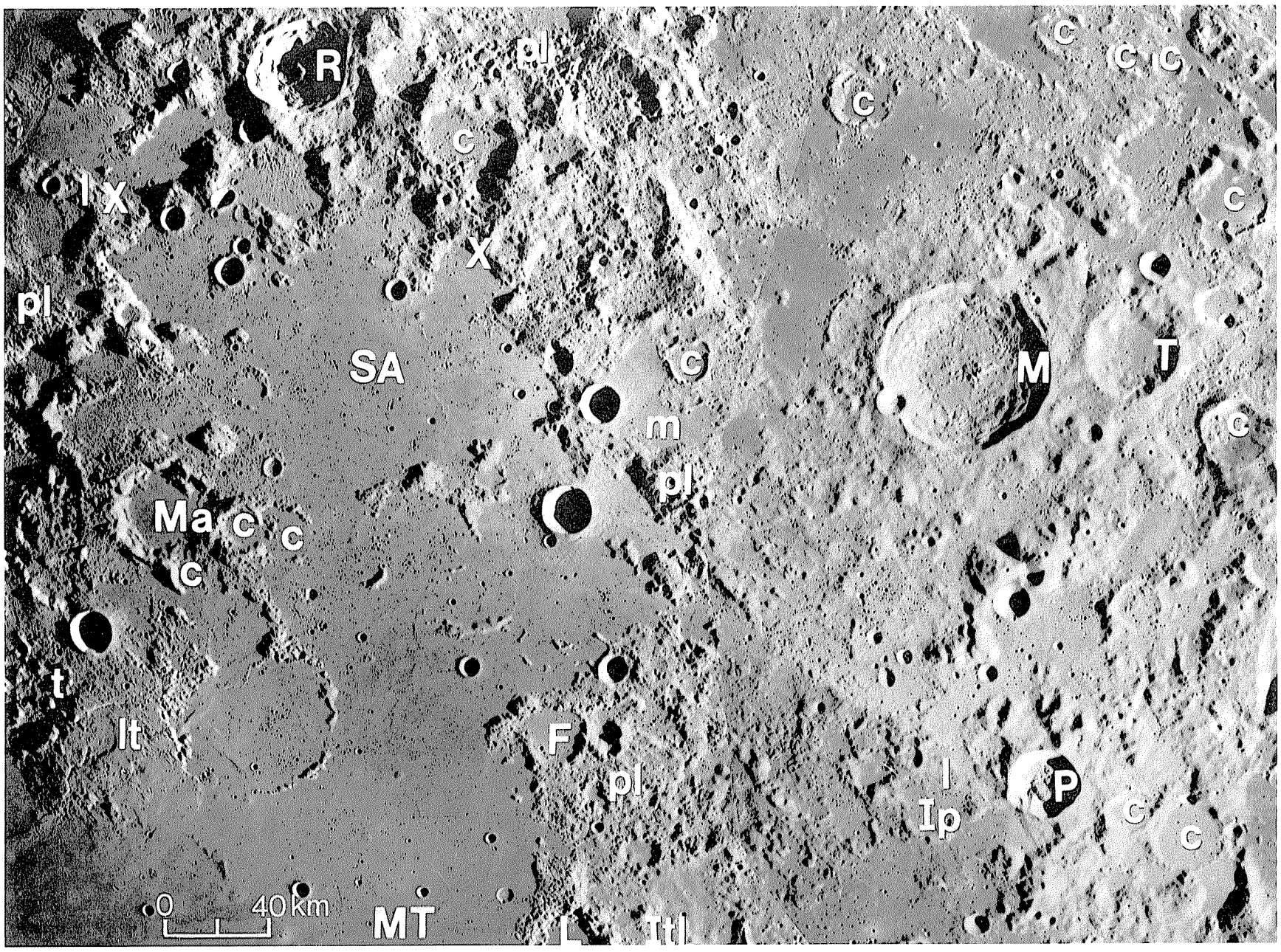
R
Rl
c
c
c
c
c
c
lX
X
c
pl
SA
c
M
T
c
m
pl
Ma
c
c
c
c
t
lt
F
pl
I
Ip
P
c
c
0
40km
MT
Ttl

A

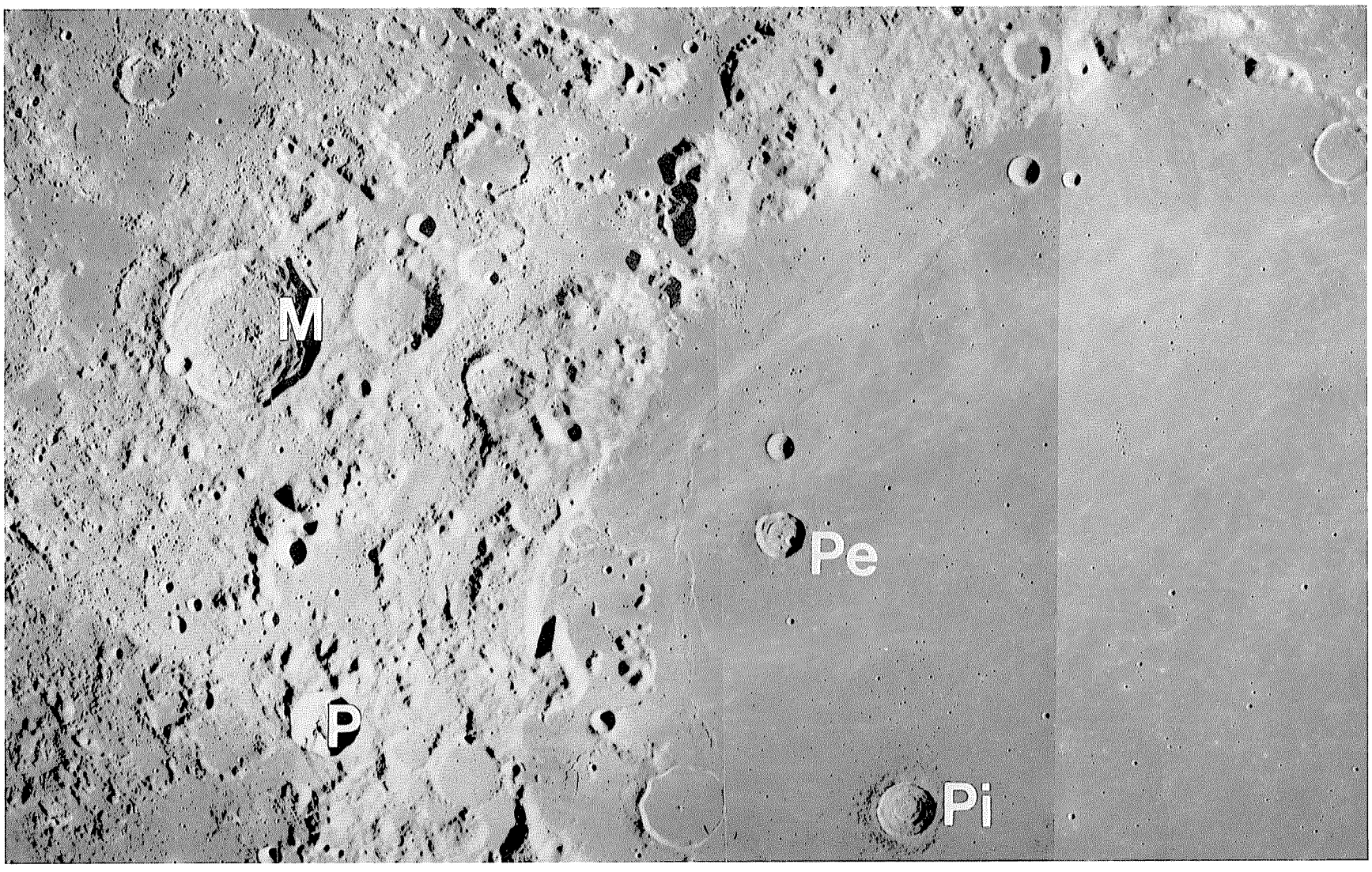
M
Pe
P
Pi

B

Relative age

Serenitatis was long considered to be an old basin because of its highly degraded appearance (Stuart-Alexander and Howard, 1970; Head, 1974b). Numerous degraded craters in the terra east of the mare were thought to be superposed on the basin (figs. 1.7, 5.17, 9.11, 9.14). The interpretation of these craters and the position of the rim are critical to the important question of the relative age of the Serenitatis basin. The clustering and nearly subequal size of some of the craters suggest an origin as secondary craters of the Imbrium basin (for example, Littrow; figs. 9.11, 9.13; Wilhelms, 1980). Almost all the other craters resemble the degraded prebasin craters visible close to the rims of the Orientale and Nectaris basins (figs. 4.4, 7.9). Therefore, these craters are older than Serenitatis, provided that the Serenitatis rim lies west of the craters near the edge of the mare. Only three primary craters larger than 20 km in diameter visible east of Serenitatis are clearly younger than Serenitatis and older than Imbrium (Kirchhoff, Maraldi, Römer A; figs. 9.11, 9.14). Le Monnier (61 km, 27° N., 31° E.; fig. 6.2*B*) also seems likely to lie in this intermediate stratigraphic position, but it is only a "ghost" crater whose age is uncertain.

Several additional lines of evidence are consistent with a relatively young age of the Serenitatis basin. (1) The near-destruction of the west sector by the Imbrium basin, a clear indicator of relative age, has no significance for absolute age; the two basins could be almost contemporaneous. (2) Serenitatis secondaries may be superposed on Crisium ejecta and the Crisium rim (figs. 9.14, 9.15; Wilhelms, 1976). (3) No Crisium ejecta is texturally evident near the Taurus-Littrow massifs (figs. 9.11, 9.13); if Serenitatis is not the younger of the two basins, the Crisium pattern of ejecta must have been highly asymmetric (which, in fact, is possible, as shown by the analogy with Messier). (4) The substantial thickness of the basalt in Mare Serenitatis indicates little filling or isostatic rebound since formation of the Serenitatis basin. (5) Apollo 17 astronaut R.E. Evans described the massifs of Serenitatis as much fresher and more boulder-strewn than those of Crisium (Evans and El-Baz, 1973, p. 16); although morphology has not proved to be a very precise age indicator for basin ages, at least this evidence helps counter reliance on Crisium's apparently fresh overall morphology as an indicator of its youth.

In summary, the roughness of the terra east of Serenitatis is due to Procellarum and Serenitatis massifs, Imbrium secondaries, Imbrium deposits (fig. 9.11), Serenitatis secondaries, and pre-Serenitatis craters. None of these features establishes an old age for the basin. A relatively young Nectarian age for Serenitatis is favored here.

FIGURE 9.11.—Mare Crisium and circum-Crisium terrain. Primary-impact craters common to both scenes include Macrobius (M; 64 km, 21° N., 46° E., Lower Imbrian) and Proclus (P; 28 km, late Copernican; compare fig. 3.33). Trough concentric with Crisium is west (left) of Macrobius. Hummocky material, possibly ejected from Crisium or Serenitatis basin, is between Proclus and Mare Tranquillitatis (MT).

A. Nectarian primary craters include Maraldi (Ma; 40 km, 19° N., 35° E.) and Tisserand (T; 37 km); Römer (R; 40 km) is Copernican. Craters labeled "c" are believed to be secondary-impact craters of Serenitatis or Imbrium basin because of compound shape, alignment with basin radials, varying, diverse morphology of ridges, grooves, and mounds, and concentration in size range 10–20 km. Deposits of Imbrian age (Ip, Itl) and fine-scale morphology indicated by other symbols (l, lt, pl, t), possibly related to Imbrium basin, are superposed on rugged features of Crisium and Serenitatis basins (Wilhelms, 1980). SA, Sinus Amoris; MT, Mare Tranquillitatis; m, other mare patches. Rugged terra along north-south midline of photograph is probably part of Procellarum basin (pl. 3). From Wilhelms (1980, fig. 19). Apollo 17 frames M–195 (right) and M–302 (left).

B. Crisium-basin massifs, continuous in west and discontinuous (but poorly illuminated) in east. Eratosthenian craters Peirce (Pe; 19 km, 18° N., 53.5° E.) and Picard (Pi; 23 km, 15° N., 55° E.) penetrate mare (see chap. 5). Mosaic of Apollo 17 frames M–274, M–278, M–281, M–286, M–289, M–293, and M–294 (from right to left).

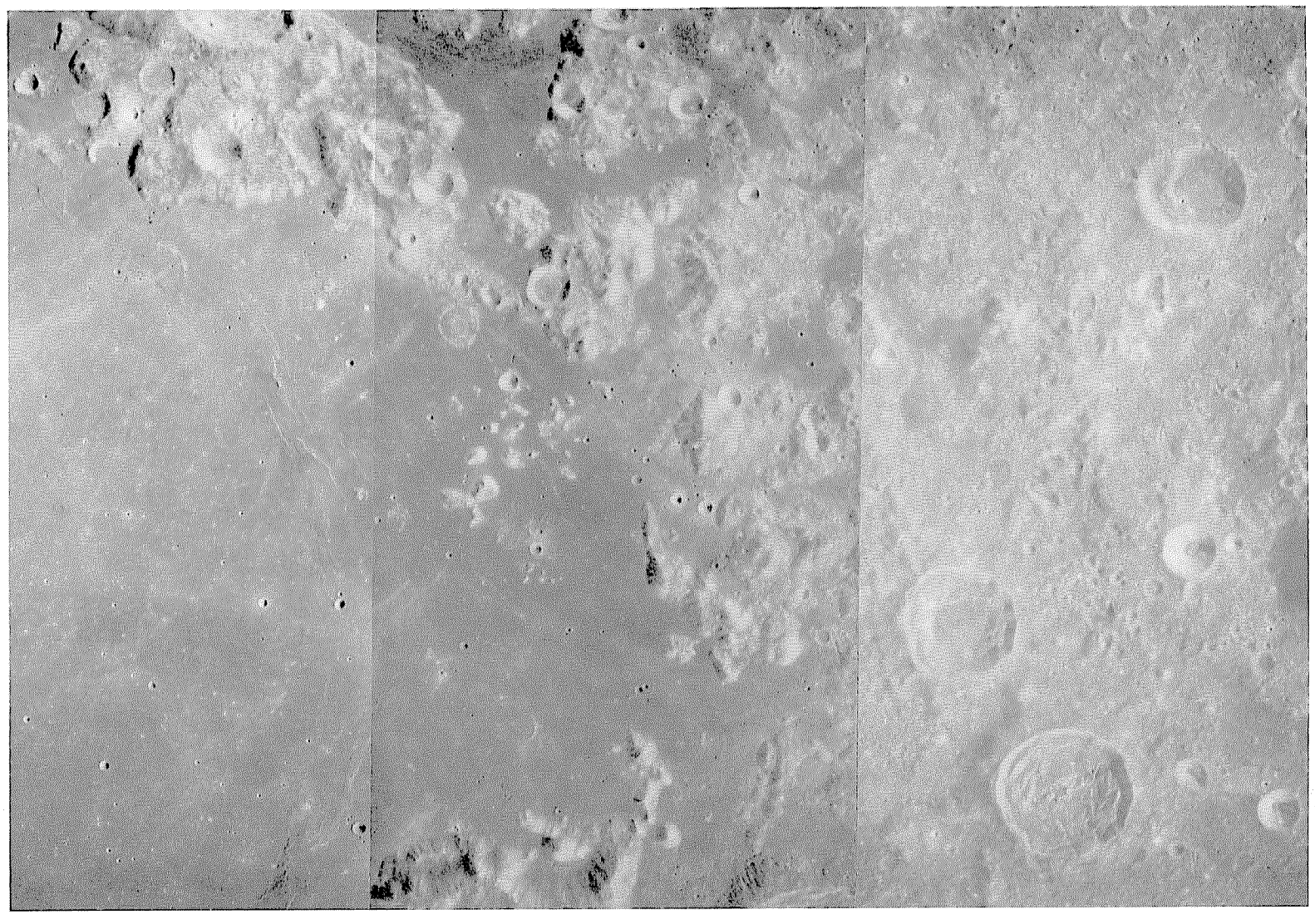

B

Petrology of Apollo 17 samples

The Apollo 17 landing site (figs. 9.16, 9.17) was chosen mainly to provide samples of terra outside strong influence of the Imbrium basin and in a known geologic context (Scott and others, 1972; Hinners, 1973). Petrologists, geochemists, and geochronologists held out the hope that primitive terra would be sampled. Geologists wanted information on basins other than Imbrium, on basin-formation processes in general, and, as always, on dates of specific events. The mare and dark-mantling materials were also to be sampled (see chaps. 5, 11), but Serenitatis-basin materials were the main objective.

Most of the sampled material is fragment-laden impact melt with a wide variety of textures but a narrow range of chemical compositions. Matrices are rich in low-K KREEP (Ryder and Wood, 1977; Winzer and others, 1977). Their prevalent textures are the types generally called poikilitic, ophitic, or subophitic, which indicate igneous-like crystallization from hot melts (fig. 9.18; Simonds and others, 1974). Other textures are aphanitic, crystallized from rapidly cooling melts (fig. 9.19; James and others, 1978). Most lithic clasts are of granulitic breccia, but clasts of Mg-suite cumulates are unusually abundant (for example, norite sample 77215 from a 2-m clast, 156-g troctolite sample 76535, and dunite sample 72415–72418; table 8.4). Many of the Mg-suite cumulates probably came from a single layered pluton (Dymek and others, 1975; Jackson and others, 1975; James, 1980). Multiple samples were collected from five melt-rock boulders, three of which were sampled at station 2 on a colluvial apron at the base of South Massif, and one each at stations 6 and 7 on basal aprons of North Massif (Dymek and others, 1976). All but one of the boulders left telltale tracks indicating their source ledges, which crop out two-thirds of the way up the massifs (fig. 9.20). Smaller samples of fragment-laden melt rock were taken from station 3, on a light-colored landslide derived from South Massif (figs. 6.1, 9.13, 9.16, 9.19). Some material of an additional terrain, the "sculptured hills," may have been collected at station 8. The sculptured hills have a hummocky surface resembling the Montes Rook Formation at Orientale or the Alpes Formation of Imbrium. The amounts collected are too small, however, to assure that they fairly represent that unit (Wolfe and others, 1981).

Emplacement process

The fragment-laden melt rocks have generally been interpreted as part of the Serenitatis-basin ejecta (Wood, 1975d; Winzer and others, 1977). This interpretation is consistent with the similarity of the massifs to those of Montes Rook, many of which are surrounded by the probably melt-rich Maunder and Montes Rook Formations (see chap. 4). The ledges presumably compose either the massifs proper or a thick superposed deposit. Superposition of Serenitatis ejecta is consistent with photogeologic observations here and at Orientale and Imbrium (figs. 4.4*E*, 10.7). However, the abundance of Imbrium-radial material in the vicinity is consistent with superposition of Imbrium ejecta on the Serenitatis massifs (fig. 9.13; Wilhelms, 1980).

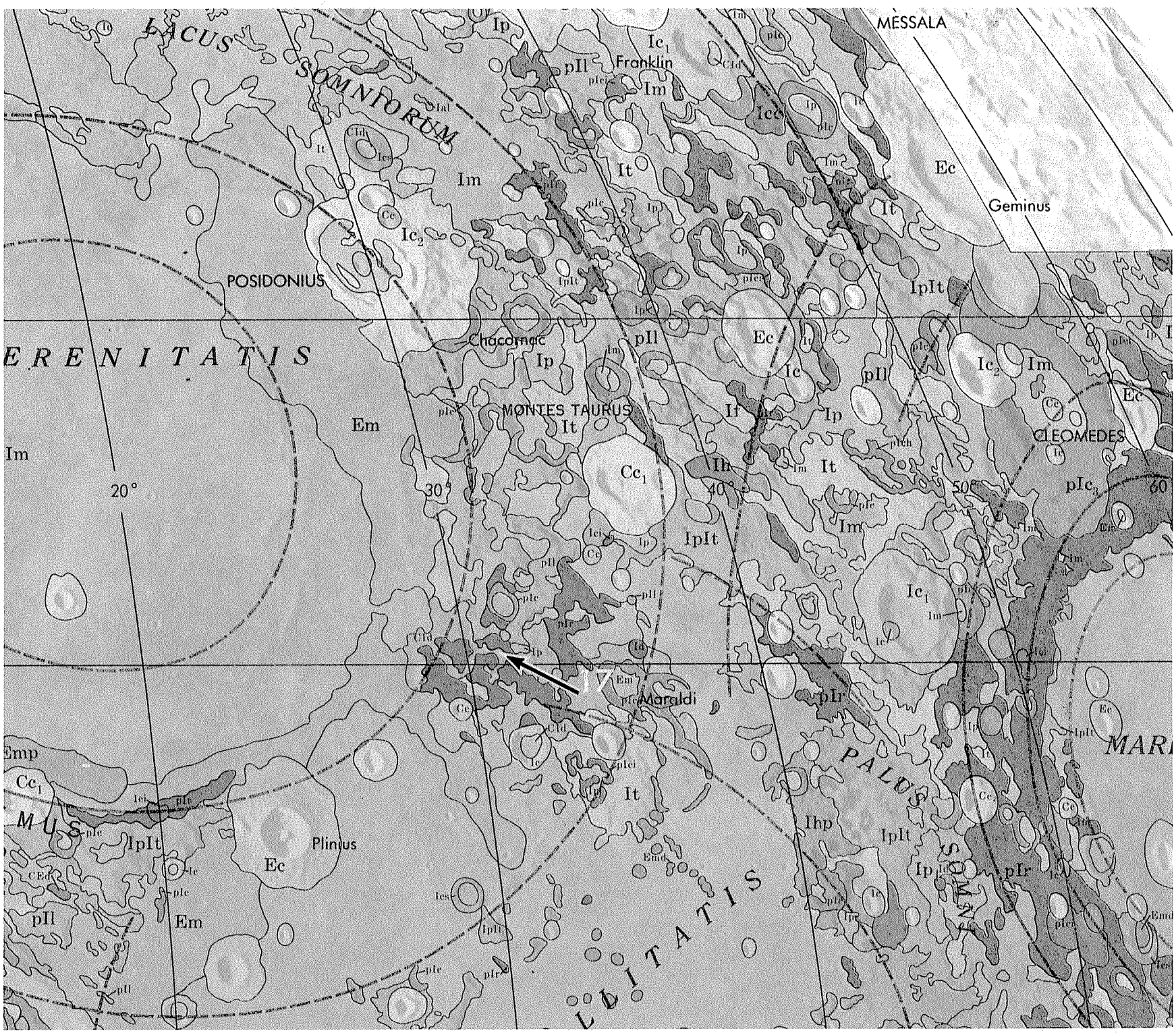

FIGURE 9.12.—Part of geologic map of nearside (Wilhelms and McCauley, 1971), including Apollo 17 landing site (arrow). Site is on unit CId, dark-mantling material of Imbrian to Copernican age, shown by mission results to be Imbrian (see chap. 11). Adjacent massifs (dark color, pIr, pre-Imbrian rugged material) are parts of Serenitatis-basin ring, interpreted here as main basin ring (table 4.1), which continues as Montes Haemus near left edge of map. Crisium-basin massifs (same color and symbol) are at right edge of map (compare fig. 9.11). Possible rings of Tranquillitatis basin are also shown. Ages of mare units (Em, Im) have been partly revised since publication of map (see chap. 11). Lower left corner of figure adjoins upper right corner of figure 9.8.

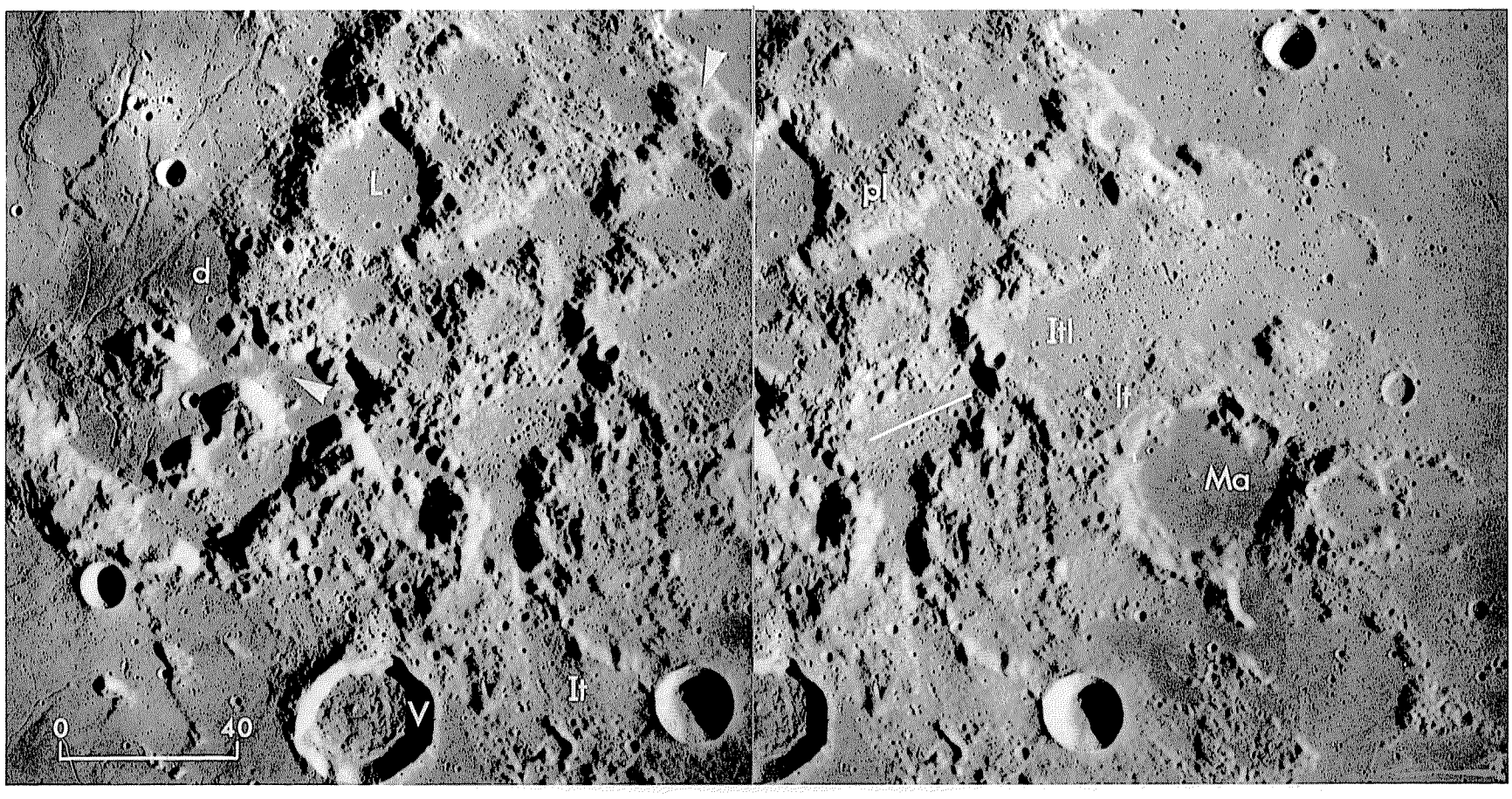

FIGURE 9.13.—Apollo 17 landing site (lower arrowhead; compare figs. 2.5*D*, 6.2*B*). South Massif is below and left of arrowhead; North Massif is above arrowhead. d, dark-mantling material. Units radial to, and believed related to, Imbrium basin (It, Itl, lt, pl; fig. 9.11*A*; Wilhelms, 1980) are superposed on much of rugged terrain but not on massifs. Lineations parallel to white line are not obviously related to any basin. L, Littrow, possible Imbrium-basin secondary crater. Ma, Nectarian crater Maraldi (compare fig. 9.11*A*); V, Upper Imbrian crater Vitruvius. Ragged line of massifs extending between Vitruvius and upper arrowhead is "Vitruvius front" (Head, 1974b). From Wilhelms (1980, fig. 18); overlaps with figure 9.11*A*. Stereoscopic pair of Apollo 17 frames M–444 (right) and M–446 (left).

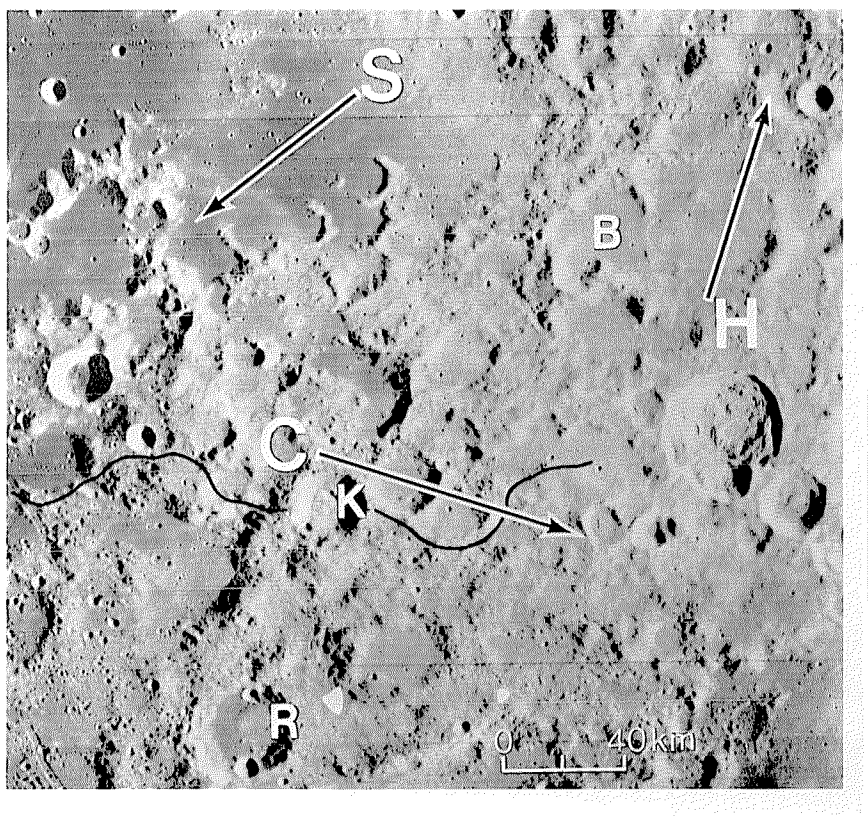

FIGURE 9.14.—Terrain northeast of Serenitatis (arrow S), northwest of Crisium (arrow C), and south-southwest of Humboldtianum (arrow H). Craters above (north of) black line are probable Serenitatis-basin secondaries, as indicated by radiality of clusters and associated linear deposits. Lineate terrain south of black line is not closely radial to any basin but is subradial to Imbrium and Crisium. Humboldtianum-basin secondary origin of irregular chain or compound craters around arrow H (including Berzelius, B) is suggested by approximate radiality. Kirchhoff (K; 25 km, 30° N., 39° E.) and Römer A (R; 35 km, 28° N., 37° E.) are probably the only post-Serenitatis, pre-Imbrian primaries in view. From Wilhelms (1976, fig. 8). Orbiter 4 frame H–74.

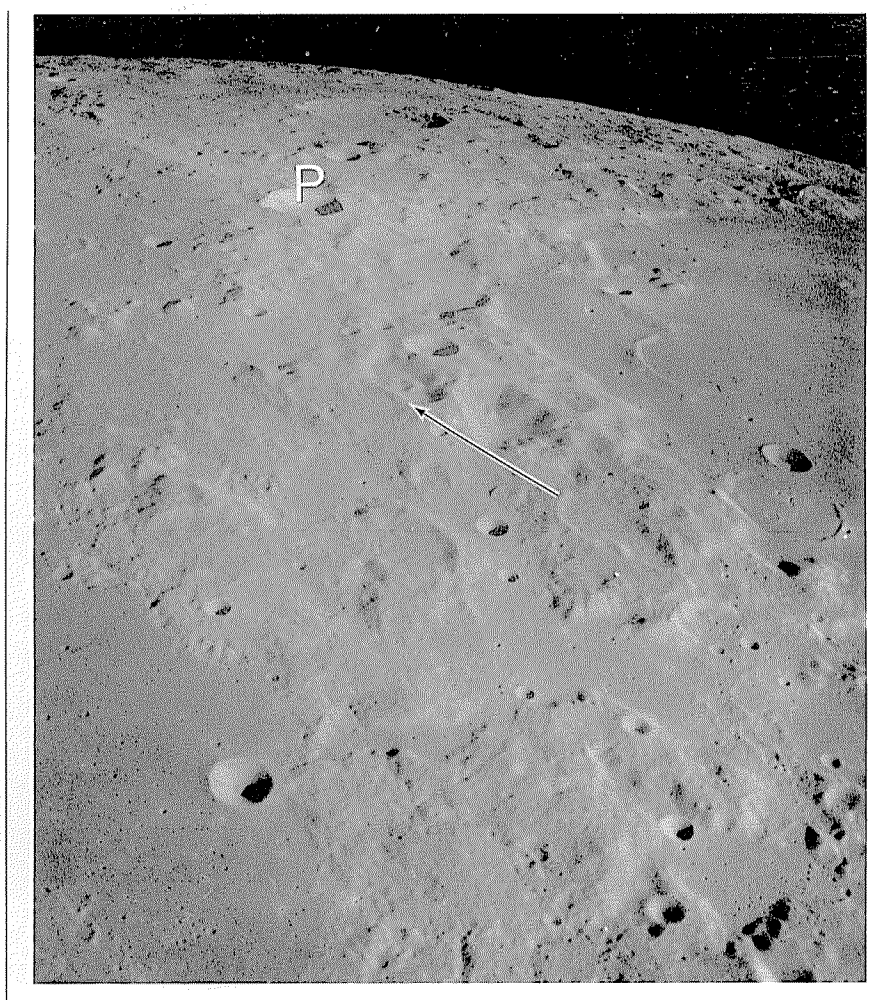

FIGURE 9.15.—Southwest rim of Crisium basin. Large crater groups aligned along arrow are probably secondaries of a basin; they are 1,000 km and 2,000 km from centers of Serenitatis and Imbrium basins, respectively. Degraded morphology favors a Serenitatis source; superposition then shows that Crisium is the older basin. P, Proclus (28 km; compare fig. 9.11). Apollo 11 frame H–6230.

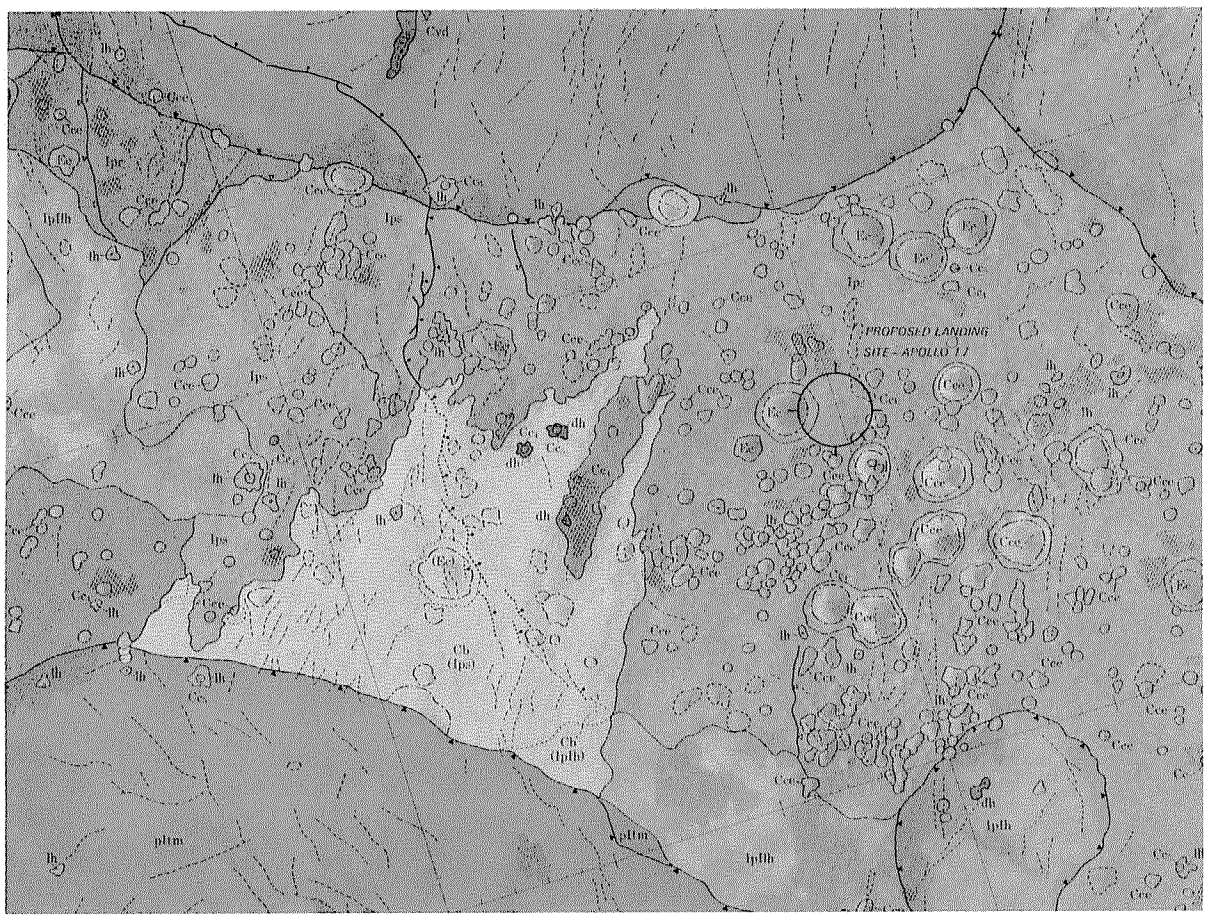

FIGURE 9.16.—Premission geologic map of Apollo 17 landing site by B.K. Lucchitta (in Scott and others, 1972). Landing took place within proposed circle. Sampled units, in order of decreasing age: pItm, pre-Imbrian terra-massif material; IpIh, Imbrian or pre-Imbrian hilly material ("sculptured hills"); Ips, Imbrian smooth plains material (subfloor basalt; see chap. 11); Ec, Eratosthenian crater material; Cce, craters now believed secondary to Tycho (chap. 13); Cb, bright Copernican material (light mantle or landslide); dh, dark-halo craters (now known to be Copernican impact craters; see chap. 13).

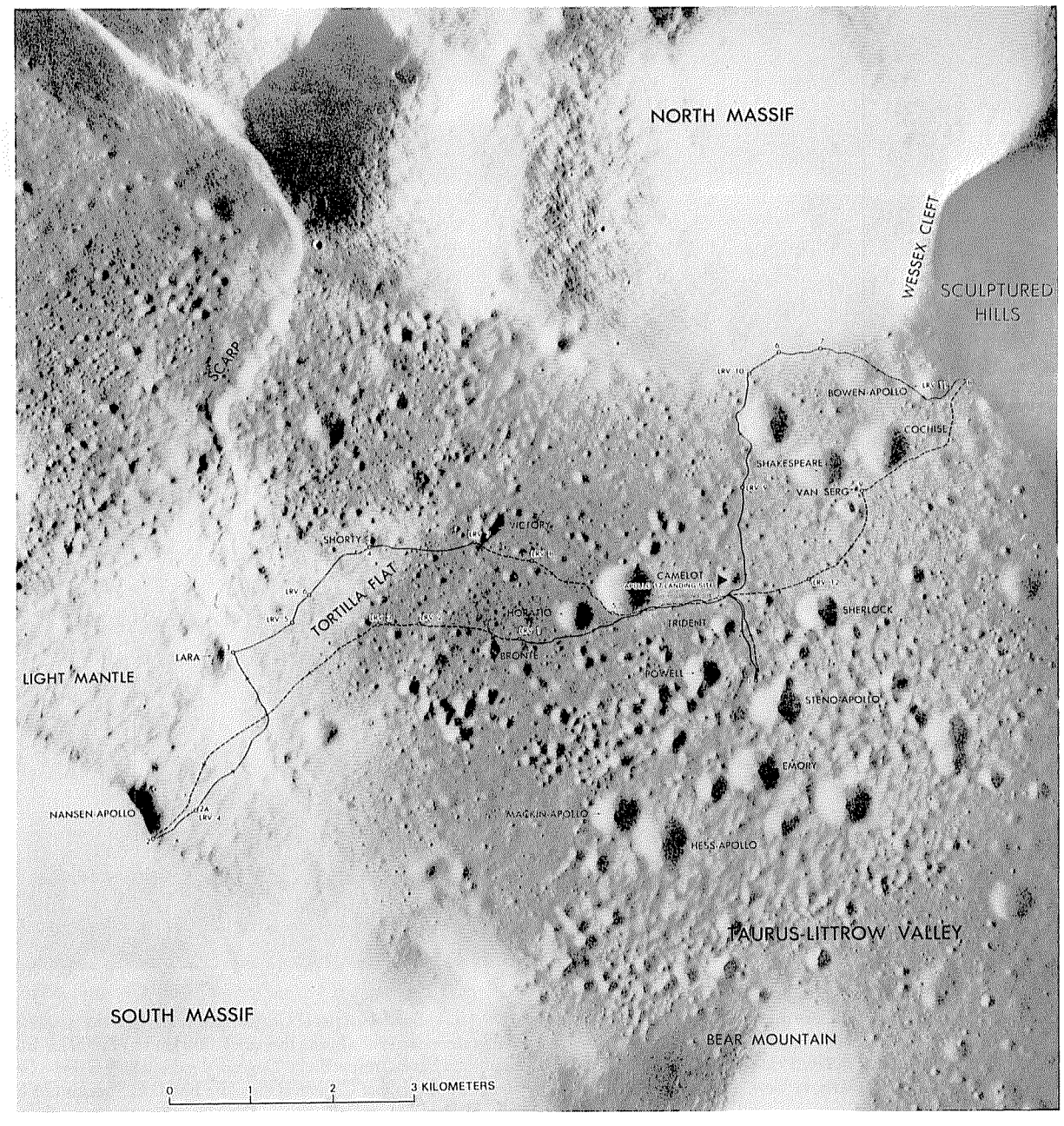

FIGURE 9.17.—Astronaut traverses and locations of sampling stations at Apollo 17 landing site.

The general chemical uniformity of the sample suite has led most of the authors cited above to conclude that the Apollo 17 samples were emplaced in a single impact, whereas others cite differences in chemistry, clast content, or apparent assembly process as evidence for multiple impacts (Ryder and others, 1975b; Chao and others, 1976; Minkin and others, 1978; Spudis and Ryder, 1981). The argument that impact melting and mixing of facies homogenize target materials of terrestrial craters (Grieve and others, 1974, 1977; Simonds and others, 1976a, b; Phinney and Simonds, 1977; Grieve and Floran, 1978) is commonly used to defend the multiple origins of lunar sample suites evaluated as "different." Extensive mixing does occur, but not total homogenization. Only the zone near the projectile is totally melted; in impacts of large, relatively slow projectiles, much additional material is incompletely melted and partly preserves the inhomogeneities of the target (see chap. 3). Furthermore, segregation of constituents according to density or volatility might create diversity during impact ejection and deposition. Therefore, the observed diversity is consistent with a Serenitatis origin for all rock-size samples collected by Apollo 17.

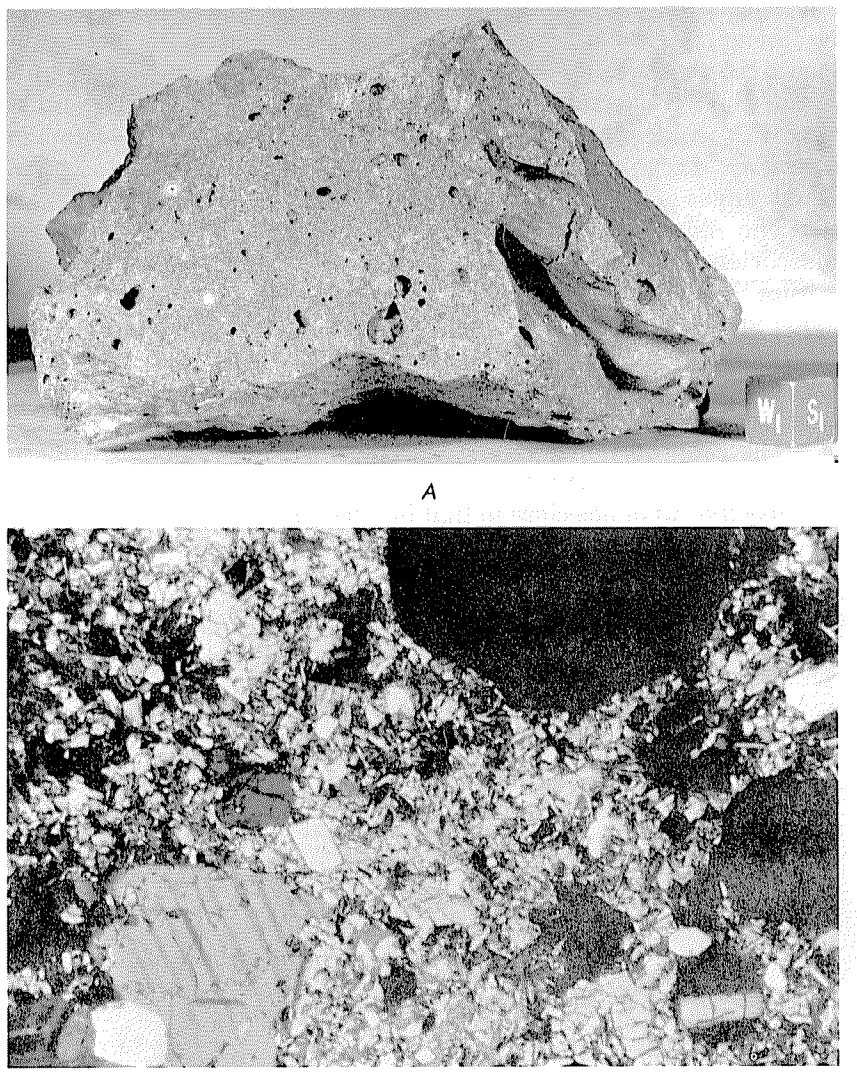

A

B

FIGURE 9.18.—Vesicular poikilitic impact melt (sample 76215) from station 6 boulder, North Massif, Apollo 17 landing site. Probably part of Serenitatis melt-rich ejecta.
A. Hand specimen. Sides of cube, 1 cm. NASA photograph.
B. Thin section of sample 76215,55. Poikilitic texture is well developed in pyroxene oikocryst (bottom center); incipient subophitic texture is around vesicles (black). Crossed polarizers; field of view, about 2 mm. Courtesy of P.D. Spudis.

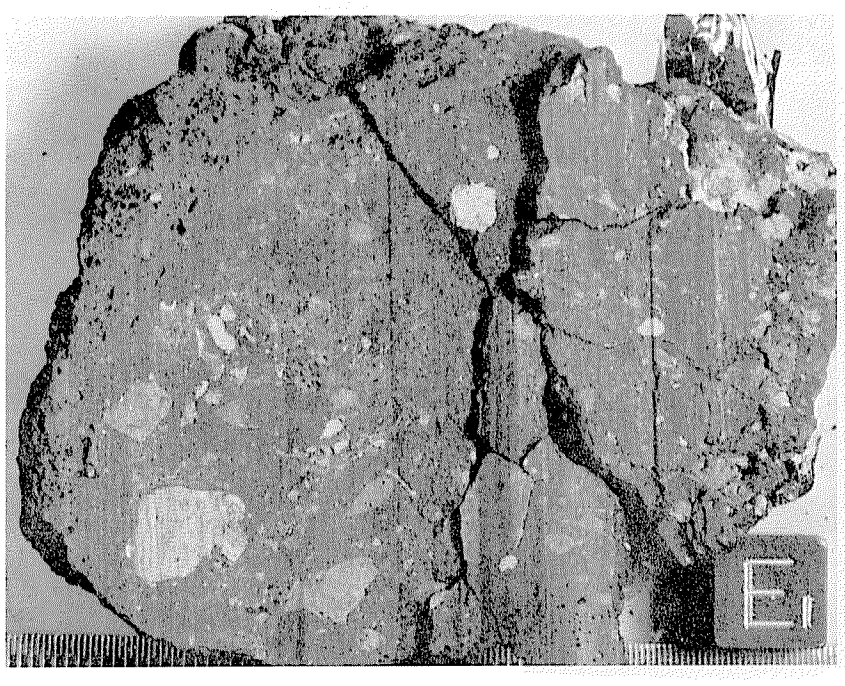

FIGURE 9.19.—Slab cut through center of aphanitic, clast-laden impact melt (sample 73255) from station 3, Apollo 17 landing site (James and others, 1978). Vesicular rind and nonvesicular interior suggest origin as melt bomb.

Absolute age

A better understanding of the geology and the availability of suitable materials have led to a clearer picture of the Apollo 17 absolute ages than for the Apollo 16 samples. The Apollo 17 ages also scatter considerably (table 9.2; Jessberger and others, 1977b, p. 2578; 1978; James and others, 1978; Wolfe and others, 1981) because of incomplete outgassing and isotopic reequilibration, as is usual in terra breccia deposits. In fact, dozens of sophisticated Ar-Ar analyses by stepwise heating of the same breccia sample (73215) yielded ages spread over 300 million years (Jessberger and others, 1977b). The laser-melting technique of determining the Ar isotopes resolved apparent age differences between parts of the same sample only 0.1 mm apart (Müller and others, 1977). However, the same careful

TABLE 9.2.—*^{40}Ar-^{39}Ar ages of Apollo 17 terra samples*

Stations (Wolfe and others, 1981): 2, at contact between light mantle (landslide) and north base of South Massif; 3, on light mantle near lower slope of Lee-Lincoln scarp; 6, on south slope of North Massif; 7, near base of North Massif, 0.5 km east of station 6.
Samples (Wolfe and others, 1981): All are from boulders or are impact-melt samples larger than 1 cm. 722-, station 2, boulder 1; 724-, station 2, boulder 3; 732-, station 3, rocks collected from rim of 10-m-diameter crater; 760-, station 6, subboulder 5; 762-, station 6, subboulder 1; 763-, station 6, subboulder 2; 77-, station 7; numbers 770-, 771-, and 772- each refer to a separate sample from a 3-m boulder.
Lithologies: Samples 72255, 73215, and 73255 are light gray, others are "blue-gray" or "green-gray"; the various colors are commonly thought to derive from different source beds.
Ages: Calculated using International Union of Geological Sciences (IUGS) decay constants (Steiger and Jäger, 1977).
References: CT76, Cadogan and Turner (1976); E79, Eichhorn and others (1979); H78, Huneke (1978); L75, Leich and others (1975); M77, Müller and others (1977); J77b, Jessberger and others (1977b); J78, Jessberger and others (1978); P75, Phinney and others (1975); S79, Staudacher and others (1979); S78, Stettler and others (1978); TC75, Turner and Cadogan (1975)

Station	Sample	Lithology	Age (aeons)	References
2	72255	Bulk fragment-laden melt rock----------	3.95±0.03	L75.
	72435	do----------	3.86±0.04	H78.
3	73215	Felsite clast----------	3.86±0.04	J77b, J78.
		Melt-derived groundmass----------	3.91±0.03	M77, J77b.
		Bulk fragment-laden melt rock----------	3.92±0.04	J77b.
		Clasts of fragment-laden melt rock-----	3.96-4.17±0.04	J77b.
	73235	Bulk fragment-laden melt rock----------	$3.90^{+0.04}_{-0.08}$	TC75.
		do----------	3.92±0.04	P75.
	73255	do----------	3.86±0.04	E79.
		do----------	3.88±0.03	J78.
		do----------	3.89-3.92±0.02	S79.
		Felsite clast----------	3.89±0.03	S79.
	73275	Bulk fragment-laden melt rock----------	3.90±0.05	TC75.
6	76015	Poikilitic melt rock----------	3.87±0.04	CT76.
		Mineral concentrates----------	3.86±0.04 to 3.90±0.06	CT76.
	76215	Poikilitic melt rock----------	3.88±0.04	CT76.
	76235	Clasts----------	3.87-3.89±0.06	CT76.
	76255	do----------	3.96±0.04	CT76.
	76275	Melt rock----------	3.96±0.04	CT76.
	76295	do----------	3.89-3.90±0.04	CT76.
	76315	Clasts----------	3.91-3.92±0.04	CT76.
		Melt rock----------	3.92±0.04	CT76.
7	77075	Melt-rock dike in large norite clast---	3.91±0.04	S78.
	77115	Bulk fragment-laden melt rock----------	3.84±0.03	S78.
	77135	Poikilitic melt rock----------	3.83±0.04	S78.
	77215	Plagioclase from norite clast----------	3.92±0.03	S78.

application of sophisticated Ar-Ar techniques that disclosed the problems also probably disclosed the youngest materials that have been completely reequilibrated—the aphanitic groundmass of a felsite clast from station 3 (sample 73255; Eichhorn and others, 1979; Staudacher and others, 1979). The age of this material is 3.87 ± 0.04 aeons.

The applicability of these precise measurements to Serenitatis has been questioned because of the uncertain provenance of the best-studied samples, which were collected at station 3 from float on the landslide and not from a known source bed, as were most of the boulders. This provenance might suggest superposition on the massifs of a post-Serenitatis deposit, possibly from Imbrium. Sample 73255 resembles a bomb that could have arrived as an isolated ballistic projectile from Imbrium or elsewhere (Spudis and Ryder, 1981). Spudis and Ryder (1981) cited the homogenization model as showing that the differences between the station 3 samples and the boulder samples are too great for both groups to have been assembled by the same impact.

The consortium responsible for studying the station 3 materials, however, considered a genetic relation of those materials to the boulder samples to be established by similar compositions (James, 1976; James and others, 1978). Moreover, one boulder sample from station 2, 72435, is coeval with the youngest age from sample 73255, 3.86 ± 0.04 aeons (Huneke, 1978). Other boulder samples yield older ages, but so do parts of the aphanatic samples, as noted. Therefore, an age of 3.86 or 3.87 aeons is accepted here as that of the Serenitatis basin. This age is consistent with tentative evidence for the relative youth of Serenitatis within the Nectarian System.

OTHER BASIN AND CRATER MATERIALS

Basins

Twelve basins, including Nectaris and Serenitatis, are considered to be of probable Nectarian age (pl. 7; table 9.3). Direct superpositional relations establish many age relations between pre-Nectarian, Nectarian, and Imbrian basins and among the Nectarian basins. An especially clear sequence is Apollo (pre-Nectarian)-Korolev (early Nectarian)-Hertzsprung (late Nectarian)-Orientale (Imbrian) (figs. 9.21*A*, *C*). Two, possibly three, age groups of Nectarian basins are recognized (table 9.3). Within a single group, the statistical error ranges of the counts of superposed craters overlap (fig. 9.22).

The older group consists of the Nectaris, Mendel-Rydberg, Moscoviense, and Korolev basins. The Nectaris deposits, which constitute the base of the Nectarian System, are very extensive and the superposed craters correspondingly numerous. The density of 79 craters at least 20 km in diameter per million square kilometers (fig. 9.22) can thus be taken as expressing the base of the system in size-frequency terms.

The deep burial by Orientale deposits of the Mendel-Rydberg basin has reduced the crater population on that basin (figs. 4.1, 4.3*R*); because the curve lies close to that for Nectaris, the Nectarian age of

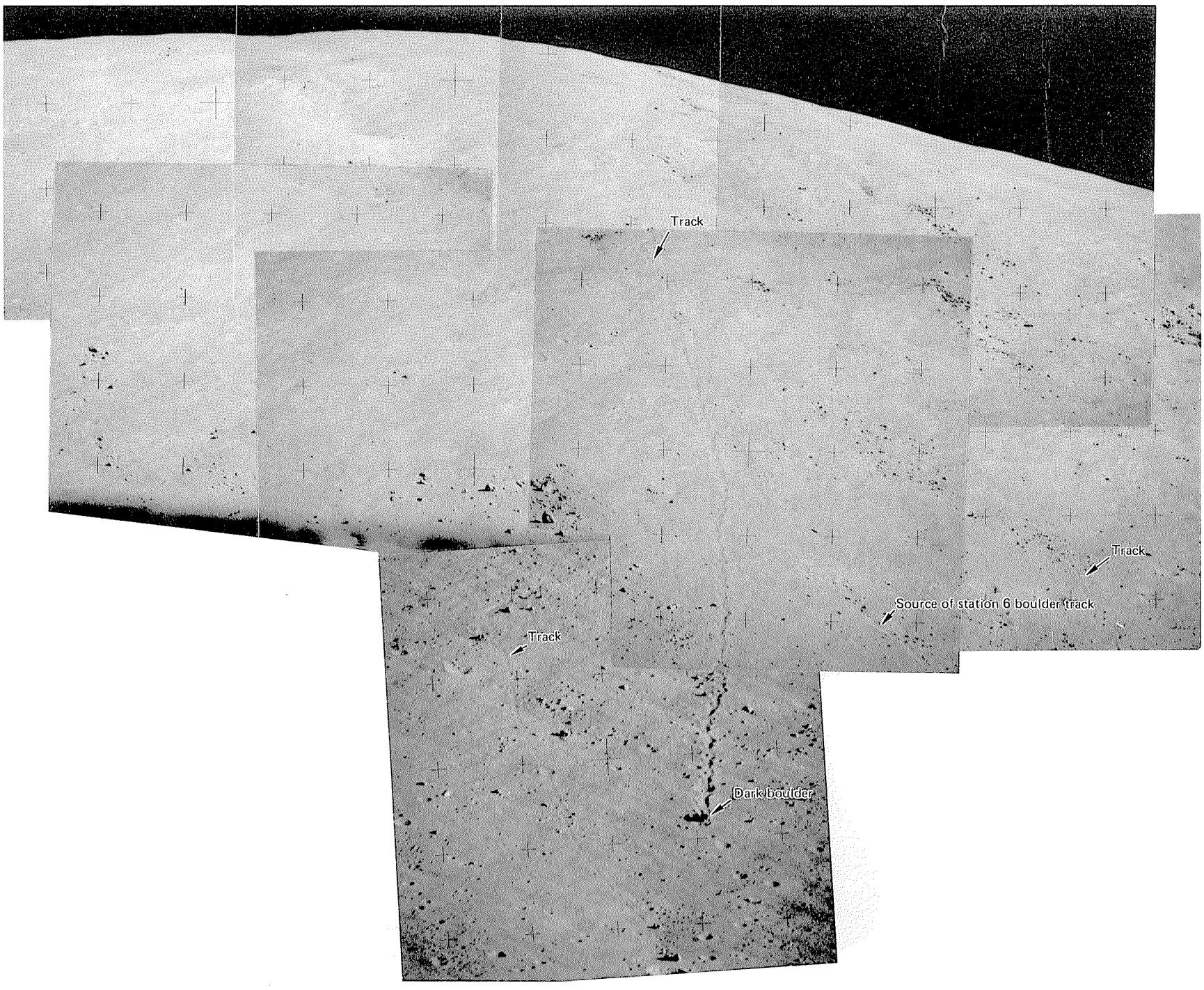

FIGURE 9.20.—Boulder tracks on North Massif (from Wolfe and others, 1981, fig. 145).

TABLE 9.3.—*Nectarian basins*

[Basins are ranked in order of increasing age; ranking is by stated density of craters or by criteria given in text; ranking of groups is more certain than ranking within a group. Diameters are from table 4.1. Parenthetical basins, existence not definitely established; parenthetical areas, buried; parenthetical densities, poor sample. Superposed craters are at least 20 km in diameter. Underlying and overlying basins determined from directly observed superpositional relations; n.d., no relations detected]

Age group	Basin	Diameter (km)	Superposed craters			Underlying basin		Superposed basin	
			Number	Area (10^6 km^2)	Density (craters/ 10^6 km^2)	Name	Figure	Name	Figure
2?	Bailly----------	300	3	(0.096)	(31)	n.d----------		Orientale----------	1.9.
2?	(Sikorsky-Rittenhouse).	310	2	(0.075)	(27)	South Pole-Aitken---	1.5	Schrödinger----------	1.5.
2	Hertzsprung------	570	51	.883	58	Korolev----------	9.21	Orientale----------	8.14, 9.21, 9.25.
						Birkhoff----------	8.14, 9.25		
						Apollo----------	8.15, 9.21		
						Lorentz----------	8.14		
						Coulomb-Sarton------	8.14, 9.25		
						(Grissom-White)-----	8.15		
						South Pole-Aitken---	9.21		
2?	Serenitatis------	740	9	.108	(83)	Crisium----------	9.11, 9.14, 9.15.	Imbrium----------	1.7, 9.11.
						Humboldtianum-------	9.14		
2	Crisium----------	1,060	45	.843	53	Humboldtianum-------	9.4	Imbrium----------	9.11.
						Smythii----------	1.5	Serenitatis----------	9.11, 9.14, 9.15.
						Lomonosov-Fleming---	---		
						Fecunditatis--------	9.5		
						Tranquillitatis-----	9.11		
						Marginis----------	9.4		
2	Humorum----------	820	24	.428	56	Nubium----------	8.10	Orientale, Imbrium---	9.23.
2	Humboldtianum----	avg 700	32	.515	62	Moscoviense---------	9.23	Imbrium----------	9.4, 10.6.
								Serenitatis----------	9.14.
								Crisium----------	9.4.
2?	Mendeleev--------	330	36	.569	63	Moscoviense, Freundlich-Sharonov, Keeler-Heaviside.	1.4	n.d----------	
1	Korolev----------	440	88	1.113	79	Freundlich-Sharonov, Apollo, South Pole-Aitken.	9.21	Orientale, Hertzsprung.	9.21.
1	Moscoviense------	445	53	.609	87	Freundlich-Sharonov.	1.4	Mendeleev----------	1.4.
								Humboldtianum--------	9.23.
1?	Mendel-Rydberg---	630	18	(0.247)	(73)	(Pingré-Hausen), South Pole-Aitken.	1.9	Orientale----------	1.9.
1	Nectaris---------	860	102	1.286	79	Mutus-Vlacq---------	8.12, 9.2	Imbrium----------	3.10, 9.2.
						Fecunditatis--------	9.2		
						Tranquillitatis-----	9.2, 11.1		
						Australe----------	1.5, 9.6		
						Werner-Airy---------	8.12		
						South Pole-Aitken---	---		

Mendel-Rydberg is doubtful. A small patch of Mendel-Rydberg ejecta apparently is exposed southwest of the basin, near the crater Fizeau (pl. 7; Wilhelms and others, 1979).

Moscoviense and Korolev ejecta or secondary craters blanket pre-Nectarian craters over distances averaging a basin diameter and extending, in salients, more than two basin diameters (pls. 3, 7; figs. 9.21*C*, 9.23). Large tracts can thus be dated relative to these basins. The southwestern ejecta of Korolev is distinctly lineate (fig. 9.21*D*). Radial alignment of some fresh secondary chains inside Korolev suggests an Orientale origin, and so the adjacent plains may also be of Orientale origin (fig. 9.21*B*). The crater densities on Korolev and Nectaris are similar, but they overlap only where the Nectaris curve is kinked. Although more craters per unit area are superposed on Moscoviense than on Nectaris, most of the surplus craters are small. The curves as a whole thus indicate that both the Korolev and Moscoviense basins are younger than Nectaris.

The definite basins of the younger group are Humboldtianum, Humorum, Crisium, and Hertzsprung. Bailly and Serenitatis are probably members of this group, although they cannot be dated reliably by superposed craters. Humboldtianum ejecta covers much of the northern part of the east lunar limb (fig. 9.4). Conspicuous radial lineations and secondary craters extend 600 km south of the topographic rim, which is a clearly defined ring 300 km in radius in this sector. An exterior arc 600 km in radius is covered by the ejecta (Wilhelms and El-Baz, 1977). Humboldtianum is a double or triple basin whose parts form a figure-8 (pl. 3; fig. 9.4; Lucchitta, 1978). A ring 150 km in radius is conspicuous in both parts of this figure-8; a poorly defined ring between the topographic rim and the 150-km-radius ring is visible in the southern part. The northern part of the figure-8 consists of irregular uplifts that do not clearly define rings (Lucchitta, 1978). Crater counts (fig. 9.22) are consistent with the age relation demonstrated by superposition of Crisium secondaries on Humboldtianum (fig. 9.4).

The Humorum basin is also irregular in most sectors (figs. 4.3*U*, 9.24). The most complete ring, 440 km in diameter, bounds Mare Humorum (table 4.1). A conspicuous and rimlike scarp almost twice as large (410 km radius) and resembling Montes Cordillera lies south of this mare-bounding ring (fig. 9.24*B*). This scarp is the topographic rim in its sector and so is here considered to be the boundary of excavation, despite lesser expression in other sectors. Although an 820-km diameter is, furthermore, consistent with the considerable extent of conspicuous deposits and secondary craters southwest of the basin (fig. 9.24*B*), this large size cannot be confirmed because Humorum deposits are buried in other sectors. Sufficient numbers of superposed craters are exposed to date Humorum as part of the younger group but not to establish its exact place in the group. Humorum and Crisium appear to be nearly contemporaneous.

The fresh-appearing Hertzsprung helps clarify the geology of the other basins (fig. 9.25). The secondary craters extend as far as 1,300 km north of the 570-km-diameter ring. This relation and the near-completeness and rimlike morphology indicate that the 570-km-diameter ring bounds the excavation (see chap. 4). The interior rings probably formed by floor deformation by the oscillatory-uplift mechanism (stage E, fig. 4.12). Hertzsprung may be the youngest Nectarian basin. Although the ends of the cumulative size-frequency curves representing small craters lie above those for Crisium and Humorum, the large-crater end lies below (fig. 9.22). The large-diameter end is considered to be more reliable because some small craters were probably missed in the counts of poorly photographed parts of Crisium and Humboldtianum.

The craterlike Mendeleev basin is surrounded by lineate ejecta and secondary craters in the well photographed southern peripheral zone (fig. 9.26*A*). Because of this morphologic freshness, it is mapped as late Nectarian on plate 7. Fairly distinct crater counts suggest, however, that Mendeleev may be intermediate in age between the two main groups.

Several factors limit the further resolution of Nectarian age differences by crater counts. The small Bailly basin, the questionable Sikorsky-Rittenhouse basin, and the extensively buried Serenitatis basin present insufficient exposed surface to be dated by superposed craters. Even for the well-exposed large basins, crater counts are statistically no more definitive than for pre-Nectarian basins because relatively few craters are available for dating the Nectarian surfaces. The statistics of some of these counts could be improved by adding craters smaller than the 20-km-diameter cutoff used to prepare figure 9.22, but the necessary primary-secondary and superposed-buried distinctions cannot be made for other, poorly photographed basins.

The inability of these criteria to distinguish between some basins may reflect natural groupings. Wetherill (1977a) suggested that large impacts might cluster in time because related projectiles derived by breakup of a single large body from the outer Solar System are consumed by collisions with the Moon and terrestrial planets in relatively brief spurts (millions or tens of millions of years). The substantial gap in crater densities between the youngest large Nectarian basin (probably Hertzsprung; fig. 9.22) and the oldest Imbrian basin (Imbrium) is strikingly suggestive of such clustering of large impacts.

Craters

Many craters can be identified as Nectarian (table 9.4), and some of these craters can be dated within the system relative to the Nectarian basins (pl. 7). Craters superposed on Nectaris-basin materials but nicked by Imbrium-secondary craters provide type examples of Nectarian crater morphology (figs. 8.5, 9.1, 9.2, 9.27). Nectarian craters larger than 20 km in diameter have generally deeper floors and rougher primary topography of rim and walls (as opposed to superposed topography) than do pre-Nectarian craters. Central peaks also are more commonly exposed in Nectarian craters, although they may be submerged if subjected to deposits from a nearby crater or basin (figs. 9.21*E*, 9.27). Some of the largest Nectarian craters have radial ejecta textures and secondary craters (fig. 8.11). Apparently, typical pre-Nectarian crater morphologies are nowhere superposed on Nectarian surfaces, except possibly for some marginal craters that appear to be superposed on outer parts of the Korolev and Moscoviense basins, here considered to be early Nectarian (fig. 9.21*D*), and for a few disputed nearside craters that could be pre-Nectarian (pl. 7). Although identifiable Nectarian craters smaller than 20 km in diameter are more numerous than identifiable pre-Nectarian craters of this size (Wilhelms and others, 1978), their morphologies vary too greatly to be useful for dating isolated craters. Their profiles range from cone-shaped to flat-floored, and their numbers appear to dwindle greatly at diameters of about 5 km because of mutual obliteration near the steady state (table 7.3).

TABLE 9.4.—*Representative Nectarian craters*

[Cross rules divide diameter ranges mapped differently in plate 7: smaller than 30 km, unmapped; 30 to 119 km, interiors mapped; 120 km and larger, exterior deposits mapped where exposed. L, long axis of elongate crater; LI?, possibly Lower Imbrian; pN?, possibly pre-Nectarian]

Crater	Diameter (km)	Center (lat)	Center (long)	Figure	Remarks
Kirchhoff-------	25	30° N.	39° E.	9.14	---
Römer A---------	35	28° N.	37° E.	9.14	---
Tisserand-------	37	21° N.	48° E.	9.11	---
Maraldi---------	40	19° N.	35° E.	6.5C, 9.11, 9.13	---
Crookes D-------	41	10° S.	163° W.	9.21	---
Young D---------	46	44° S.	52° E.	8.5	Typical.
Mercator--------	47	29° S.	26° W.	6.9	---
Playfair--------	48	24° S.	8° E.	9.27	---
Schiller C------	49	55° S.	49° W.	7.6	---
Kohlschütter----	53	14° N.	154° E.	5.2	---
Timiryazev------	53	6° S.	147° W.	9.21	Post-Hertzsprung, LI?
Epigenes--------	55	68° N.	5° W.	10.15	---
Korolev M-------	58	9° S.	157° W.	9.21	---
Congreve--------	58	0°	167° W.	9.21	Relatively old.
Congreve U------	59	0.5° N.	171° W.	9.21	Relatively young.
Mechnikov-------	60	11° S.	149° W.	9.21	Pre-Hertzsprung.
Lebidinskiy-----	62	8° N.	164° W.	9.21	Relatively young.
Sechenov--------	62	7° S.	143° W.	9.21	Pre-Hertzsprung.
Abulfeda--------	65	14° S.	14° E.	3.16B	Typical.
Al-Khwarizmi----	65	7° N.	106° E.	8.11	Do.
Adams-----------	66	32° S.	68° E.	9.5	---
Steinheil-------	67	49° S.	47° E.	8.5	Typical.
Rheita----------	70	37° S.	47° E.	8.5, 9.1	Do.
Berosus---------	74	34° N.	70° E.	9.4	---
Aliacensis------	80	31° S.	5° E.	3.26, 9.27	Typical.
Zhukovskiy------	81	8° N.	167° W.	9.21	Relatively old.
Pitiscus--------	82	50° S.	31° E.	9.2	Typical.
Mersenius-------	84	22° S.	49° W.	9.24A	Do.
Metius----------	88	40° S.	43° E.	8.5	Do.
Rocca-----------	90	13° S.	73° W.	4.4F	LI?, pN?
Inghirami-------	91	48° S.	69° W.	4.4G, 10.42	---
Pontecoulant----	91	59° S.	66° E.	9.5, 9.6	Typical.
Kibal'chich-----	93	3° N.	147° W.	9.21	Post-Hertzsprung, LI?
Pitatus---------	97	30° S.	14° W.	1.8, 6.13D, 10.30	Atypical.
Hevelius--------	106	2° N.	67° W.	4.4H, 6.21	Faulted.
Carnot----------	117	52° N.	144° W.	8.14	pN?
Alphonsus-------	119	15° S.	2° W.	1.8, 5.10F, 7.7, 10.27	---
Chaplygin-------	124	6° S.	150° E.	1.4	Typical.
Endymion--------	125	54° N.	57° E.	9.3, 9.4	Mare fill.
Cleomedes-------	126	28° N.	56° E.	9.3	Floor fractured.
Fleming---------	130	15° N.	110° E.	1.2, 8.13, 9.28	Typical.
Albategnius-----	136	11° S.	4° E.	1.8, 10.27-10.29, 10.36	---
Neper-----------	137	9° N.	85° E.	9.4	Typical.
Longomontanus---	145	50° S.	22° W.	4.6A	---
Hilbert---------	170	18° S.	108° E.	1.2, 1.3, 8.11	---
Gauss-----------	177	36° N.	79° E.	1.2, 4.2D, 9.4	Floor fractured.
Clavius---------	225	58° S.	14° W.	4.2H, 4.6A	Typical.
Van de Graaff---	234(L)	27° S.	172° E.	1.4, 3.14B, 10.32	Double, pN?
Schwarzschild---	235	71° N.	120° E.	4.21, 10.6	Ring arcs.

Plate 7 shows a total of 560 unburied Nectarian craters larger than 30 km in diameter within a total area, covered by both pre-Nectarian and Nectarian deposits, of 19.53×10^6 km^2. As expected from stratigraphic relations, the crater density is higher on the pre-Nectarian terrane than on the Nectarian basin deposits (35 versus 22 craters/10^6 km^2, respectively). The density on the pre-Nectarian terrane is the maximum Nectarian density; extrapolating it to the whole Moon (area, 38×10^6 km^2) indicates that a total of 1,330 craters at least 30 km in diameter were formed during the Nectarian Period. If the number of Nectarian basins is 12, 111 such craters were formed between each basin impact; if there are 10 basins (excluding Mendel-Rydberg and Sikorsky-Rittenhouse), 133 such craters per basin were formed.

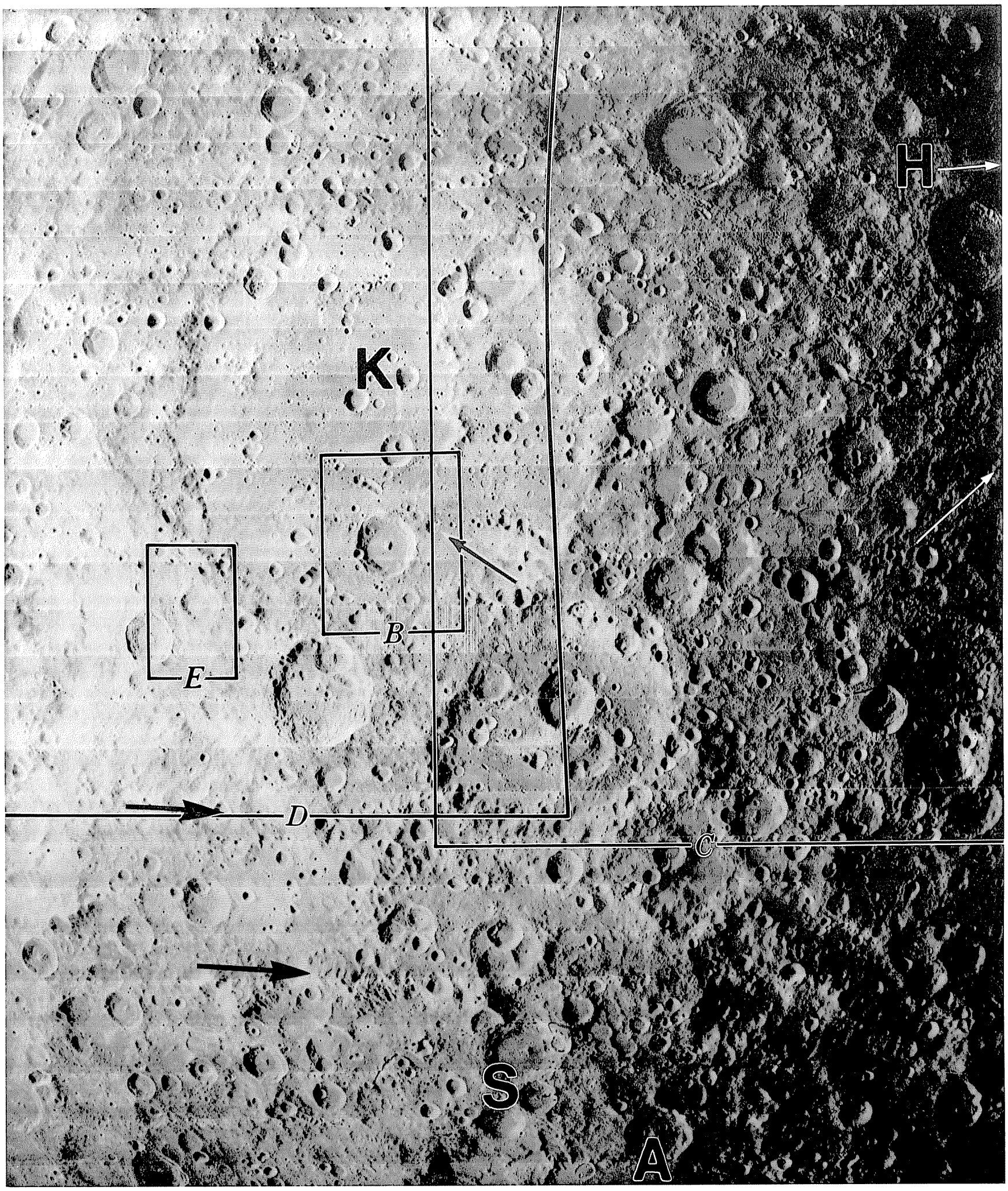

FIGURE 9.21.—Stratigraphic relations of lower Nectarian Korolev basin.

A. Korolev (K), massifs of ancient pre-Nectarian South Pole-Aitken basin (black arrows indicate massifs in fig. 8.9), northern interior of upper pre-Nectarian Apollo basin (A; letter athwart Nectarian crater Barringer, 69 km, 28° S., 150° W.), and deposits of upper Nectarian Hertzsprung basin (H; centered in direction of white arrows). Massifs near antipode of Serenitatis basin (S) are grooved, as near Orientale and Imbrium antipodes (see chap. 10); however, grooves may be secondary craters of Korolev, Hertzsprung, and Apollo. Areas of *B* through *E* are outlined; black-and-white arrow indicates chain shown in *B* and is subradial to Orientale basin. Orbiter 1 frame M–28.

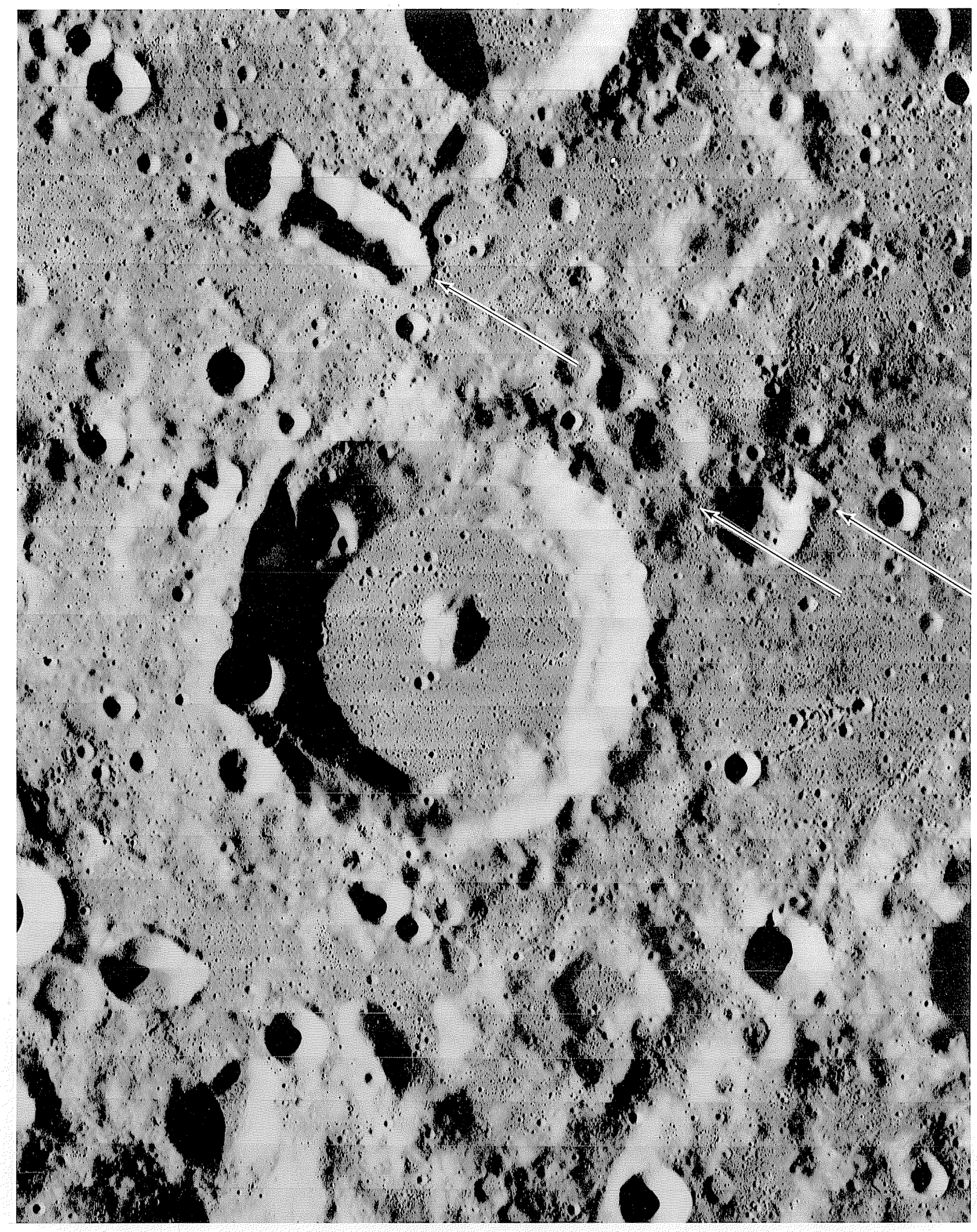

B. Detail inside Korolev basin, showing probable Orientale-basin secondary chain and fine Orientale-radial lineations. Large crater is Korolev M (58 km, 9° S., 157° W., Nectarian), filled by Imbrian plains deposits. Orbiter I frame H–38.

C. Enlargement of part of *A*, showing stratigraphic relations of Korolev and Hertzsprung basins and adjacent craters. Degradation of pre-Nectarian craters such as Galois (G; 207 km), Paschen (P; 133 km), and Tsander (Ts; 171 km) indicates burial by both Korolev and Hertzsprung deposits. Such Lower Nectarian craters as Mechnikov (M; 60 km) and Sechenov (S; 62 km) are too sharp to be older than nearby Korolev but are clearly overlain by Hertzsprung-basin secondary craters (trending northeast-southwest). Such fresh-appearing upper Nectarian craters as Kibal'chich (K; 93 km) and Timiryazev (Ti; 53 km) are superposed on Hertzsprung deposits. Sharp Orientale-basin secondaries (Iosc) cross all other units.

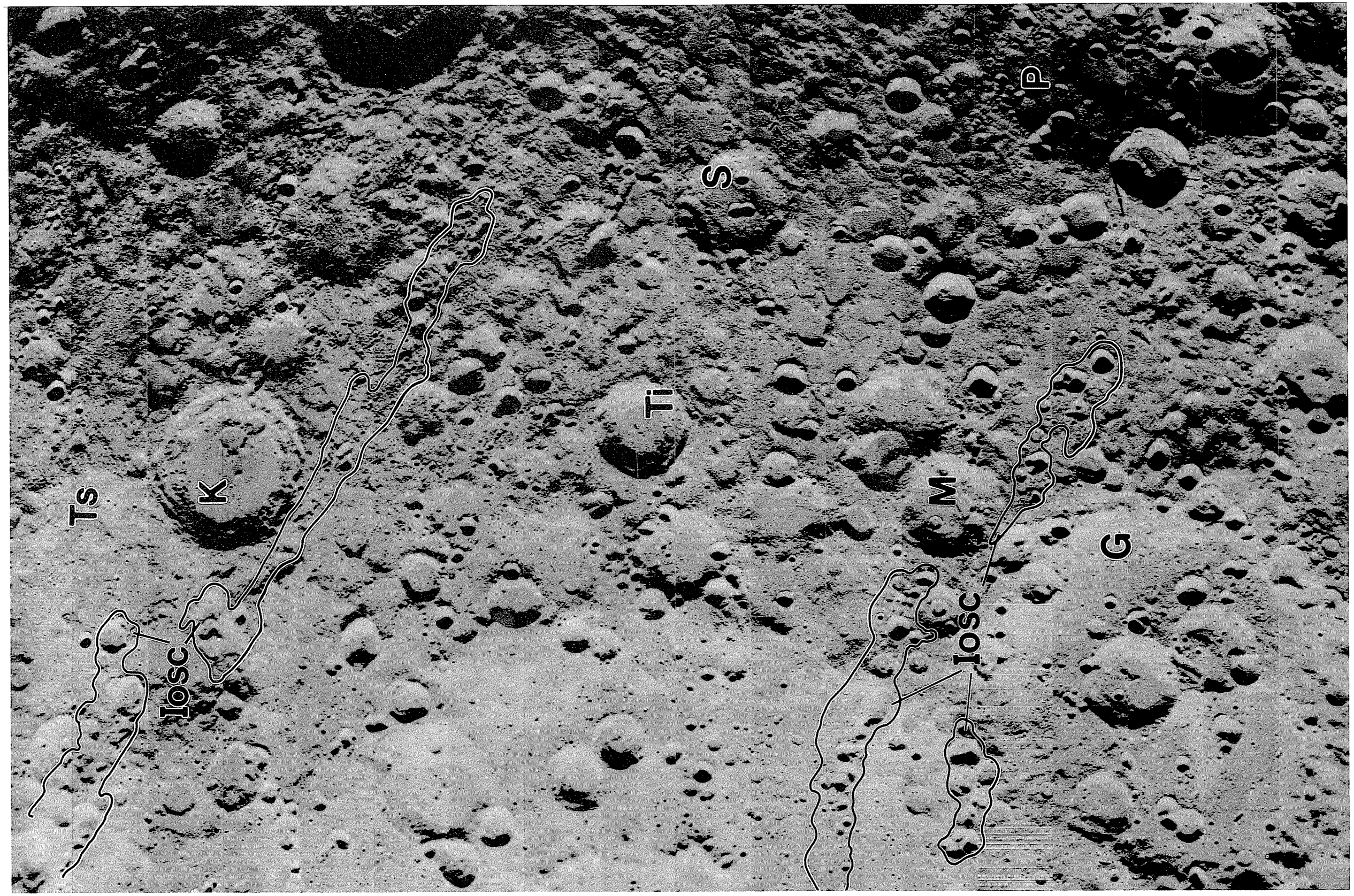
P
S
Ti
M
G
K
Ts
Iosc
Iosc

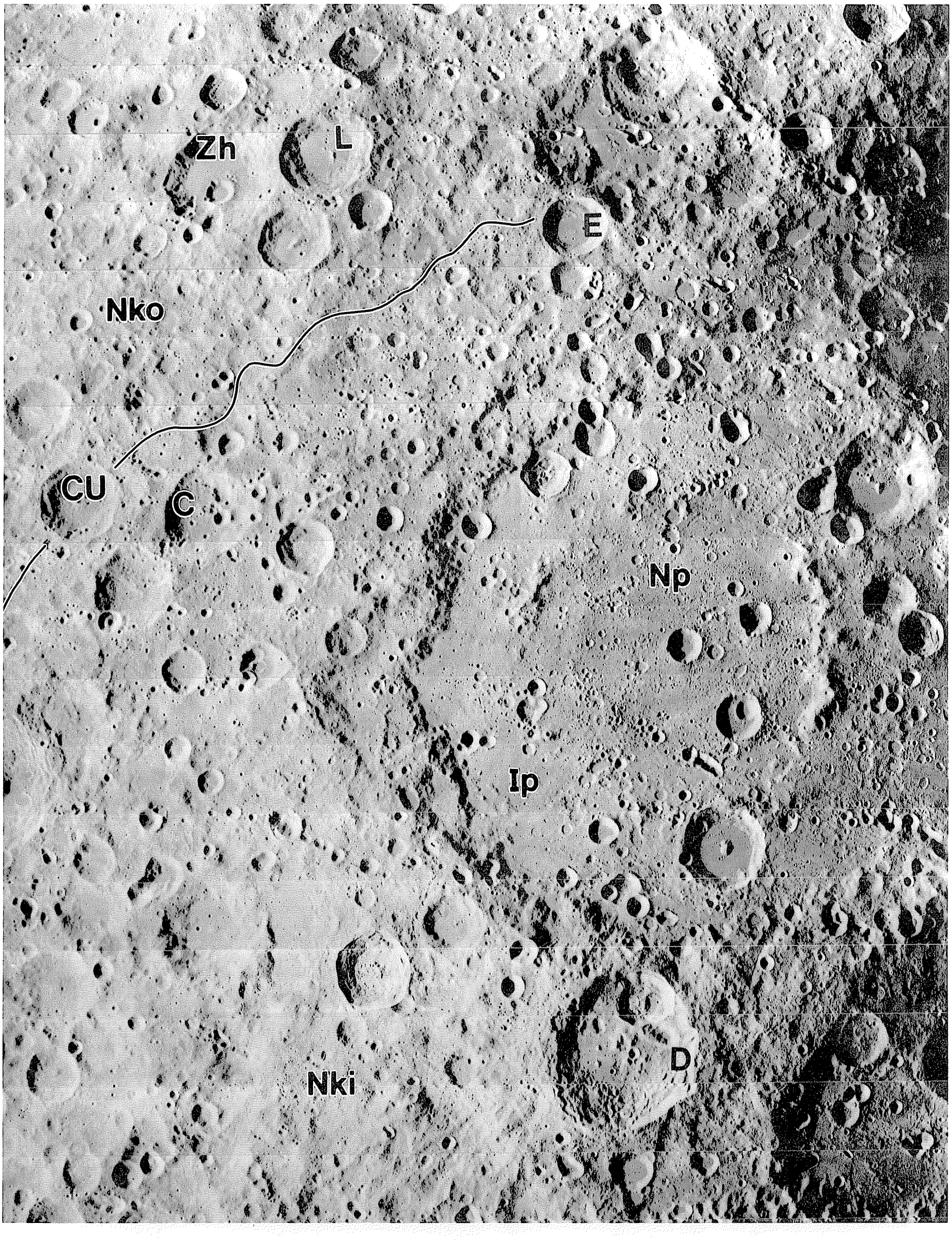

D. Korolev basin and part of periphery. Line separates inner Korolev ejecta (Nki; clearly radial southwest of basin) from outer deposits containing many secondary craters (Nko). Fresh-appearing Nectarian craters superposed on Korolev include Congreve U (CU; 59 km, 0.5° N., 171° W.) and Lebedinskiy (L; 62 km); sharper Engelhardt (E; 43 km) may be Lower Imbrian. Congreve (C; 58 km) and Zhukovskiy (Zh; 81 km, 8° N., 167° W.) are degraded Nectarian craters superposed on Korolev deposits but have morphologies and crater densities resembling those of pre-Nectarian craters. Sharply textured Doppler (D; 100 km, 13° S., 160° W.) is probably Lower Imbrian. Most plains inside Korolev are Nectarian (Np), but some lightly cratered patches are Imbrian (Ip), possibly of Orientale origin. Np and Ip may overlie basalt flows. Orbiter 1 frame M–38.

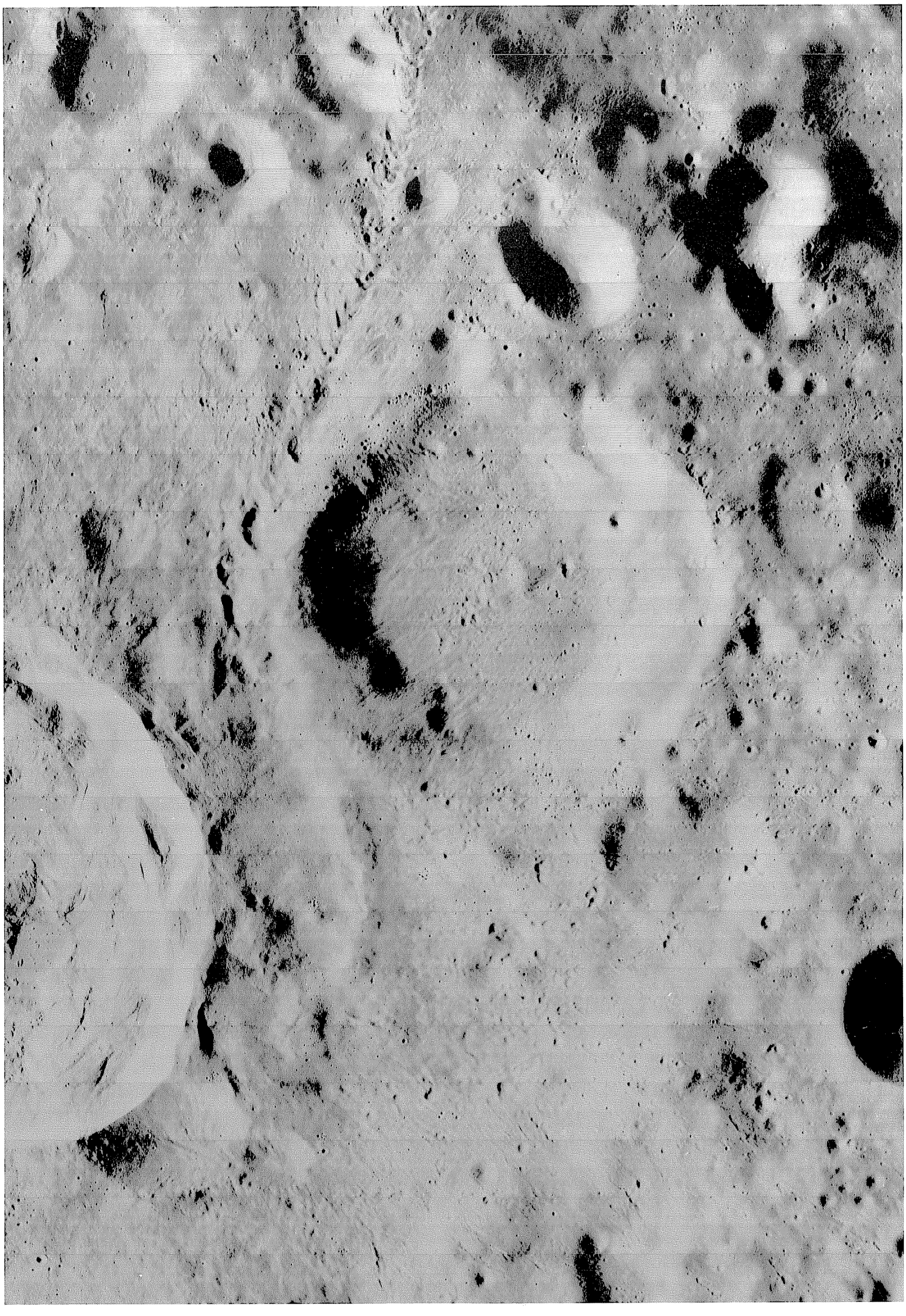

E. Crookes D (center; 41 km), overlain by deposits of Crookes (49 km, 10° S., 165° W., truncated by left edge). Superposition of Crookes D on Korolev demonstrates a Nectarian age; however, subdual because of partial burial, especially of rim sector nearest Crookes, would otherwise suggest a pre-Nectarian age. Freshness of Crookes indicates a Copernican age. Orbiter 1 frame H–30.

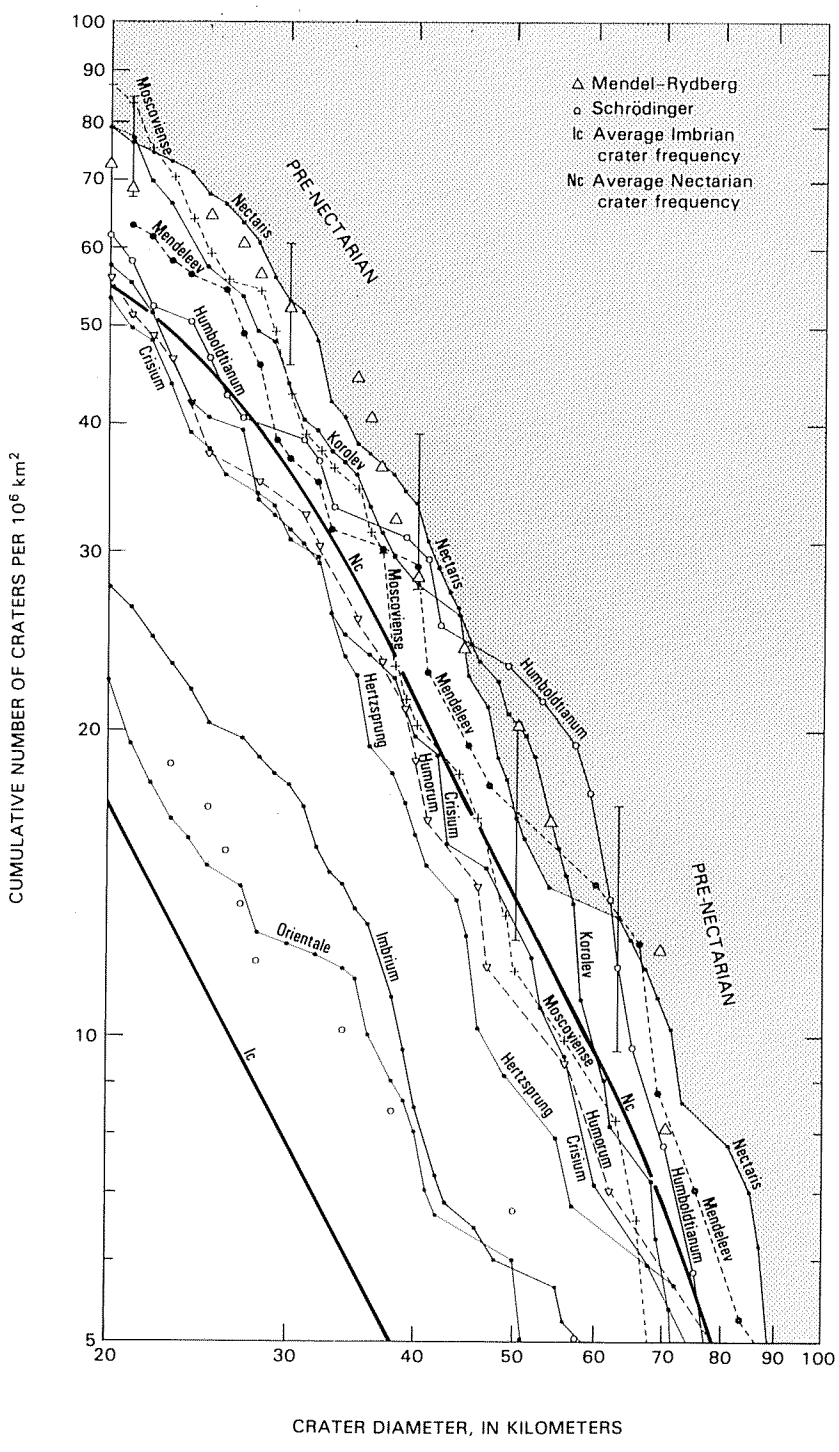

FIGURE 9.22.—Cumulative frequency distributions of craters at least 20 km in diameter superposed on Nectarian and Imbrian basins. Part of pre-Nectarian field (fig. 8.6) is in upper right. Curves for Nectarian and Imbrian craters (Nc and Ic) are from Wilhelms and others (1978). Error bars (constructed as in fig. 8.6) are for Nectaris basin; others are larger and omitted for clarity.

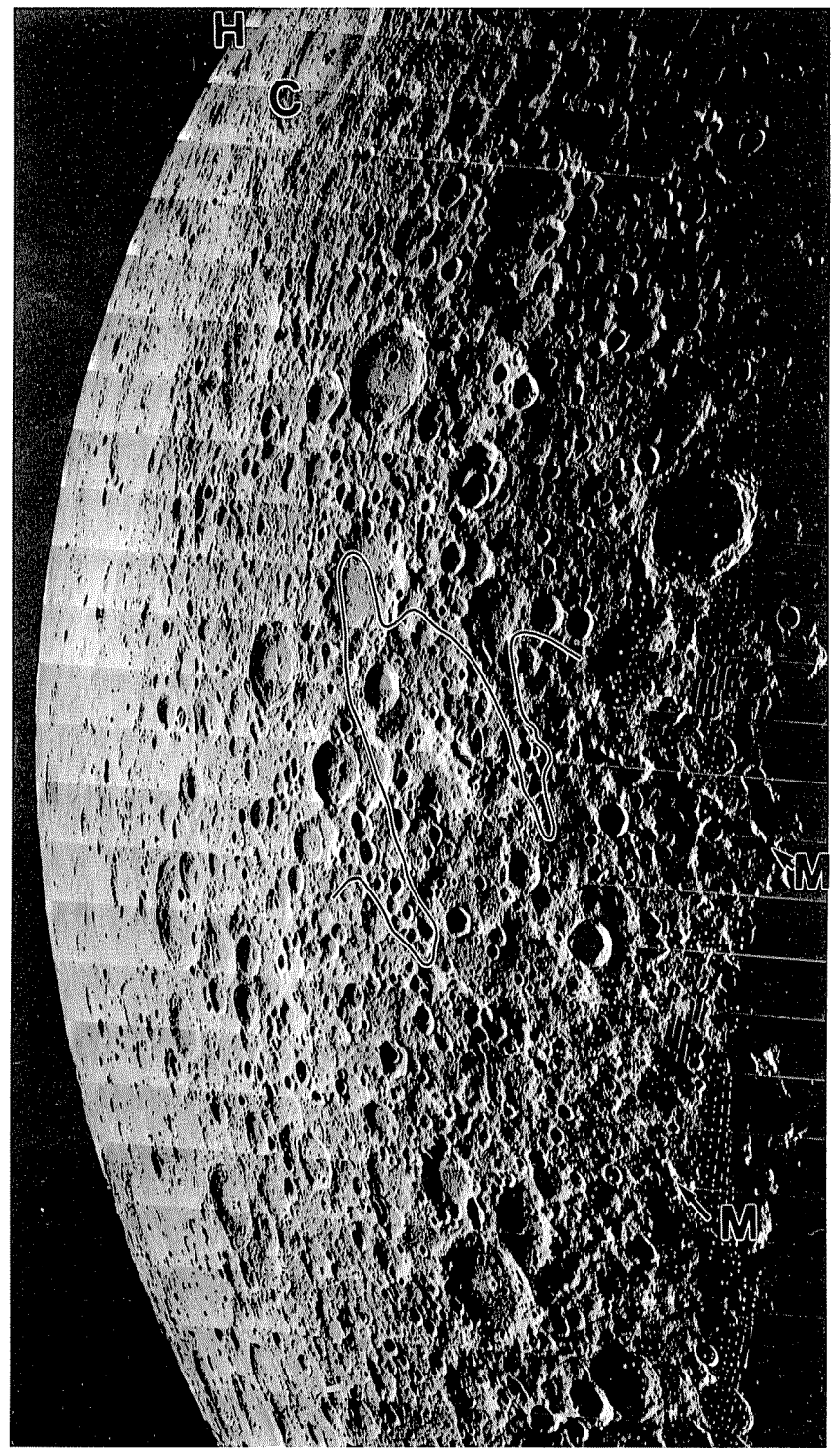

FIGURE 9.23.—Secondary-crater chains of upper Nectarian Humboldtianum basin (H, Mare Humboldtianum, outlined) truncate chains subradial to early Nectarian Moscoviense basin (M; arrows just inside shadowed basin rim). Because deposits thin away from source basins, visible large pre-Nectarian craters are less numerous near basins than in belt midway between them. C, Compton (162 km, 56° N., 105° E., Lower Imbrian). Orbiter 5 frame M–158.

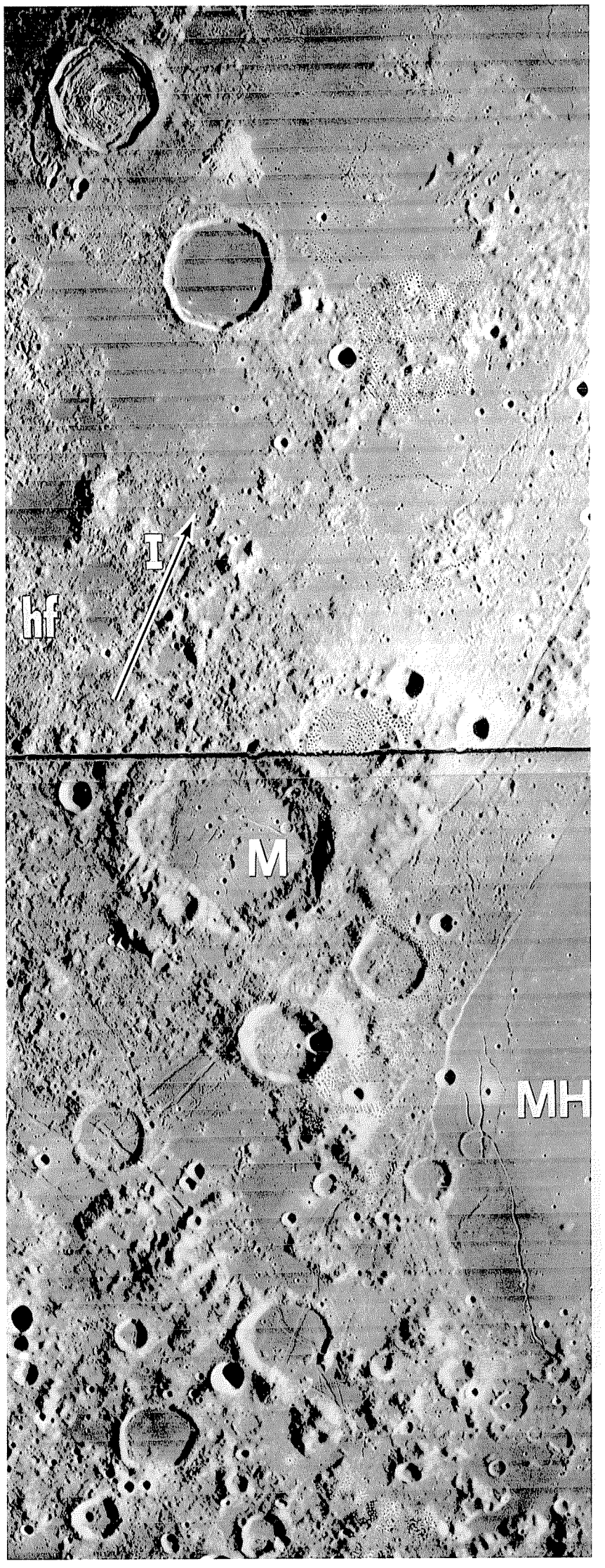

FIGURE 9.24.—Upper Nectarian Humorum basin. MH, Mare Humorum.

A. Hilly and furrowed terrain (hf) is probably a composite of Humorum basin ejecta, Imbrium-basin secondary pits and lineations, and, possibly, thin Orientale deposits; arrow (I) is radial to Imbrium. Nectarian crater Mersenius (M; 84 km, 22° S., 49° W.) is superposed on Humorum basin but is marked by Imbrium-radial lineations. Humorum-basin massifs are conspicuous south of (below) Mersenius. Orbiter 4 frame H–149.

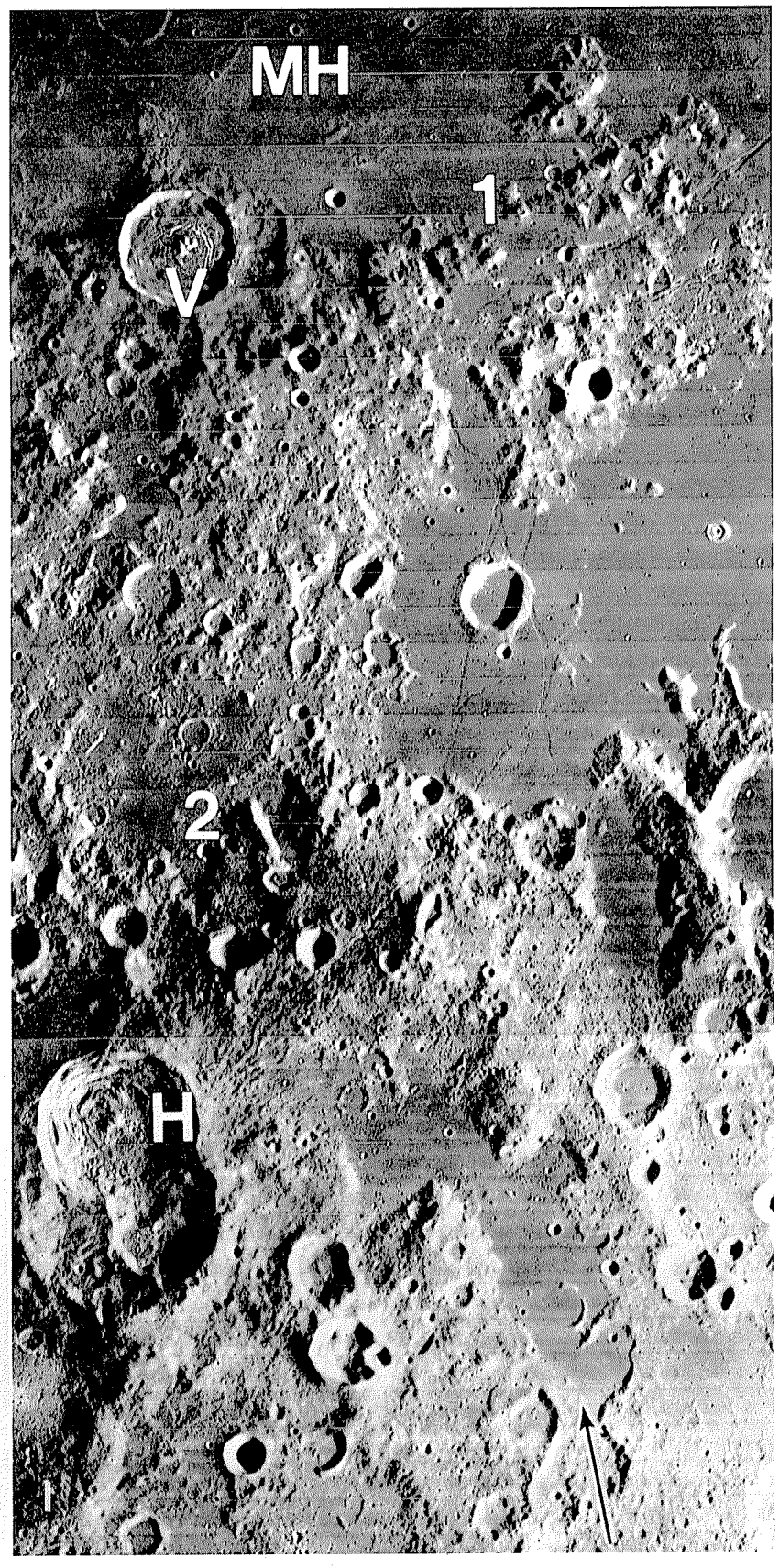

B. Terrain south-southeast of Humorum, centered in direction of arrow. Arrow marks probable secondary-impact craters of Humorum, including a subradial valley resembling Vallis Bouvard (compare fig. 4.4*D*). Major scarps of Humorum are at 1 and 2. H, Hainzel A (53 km, 40° S., 34° W., Eratosthenian); V, Vitello (42 km; see chap. 6). Orbiter 4 frame H–136.

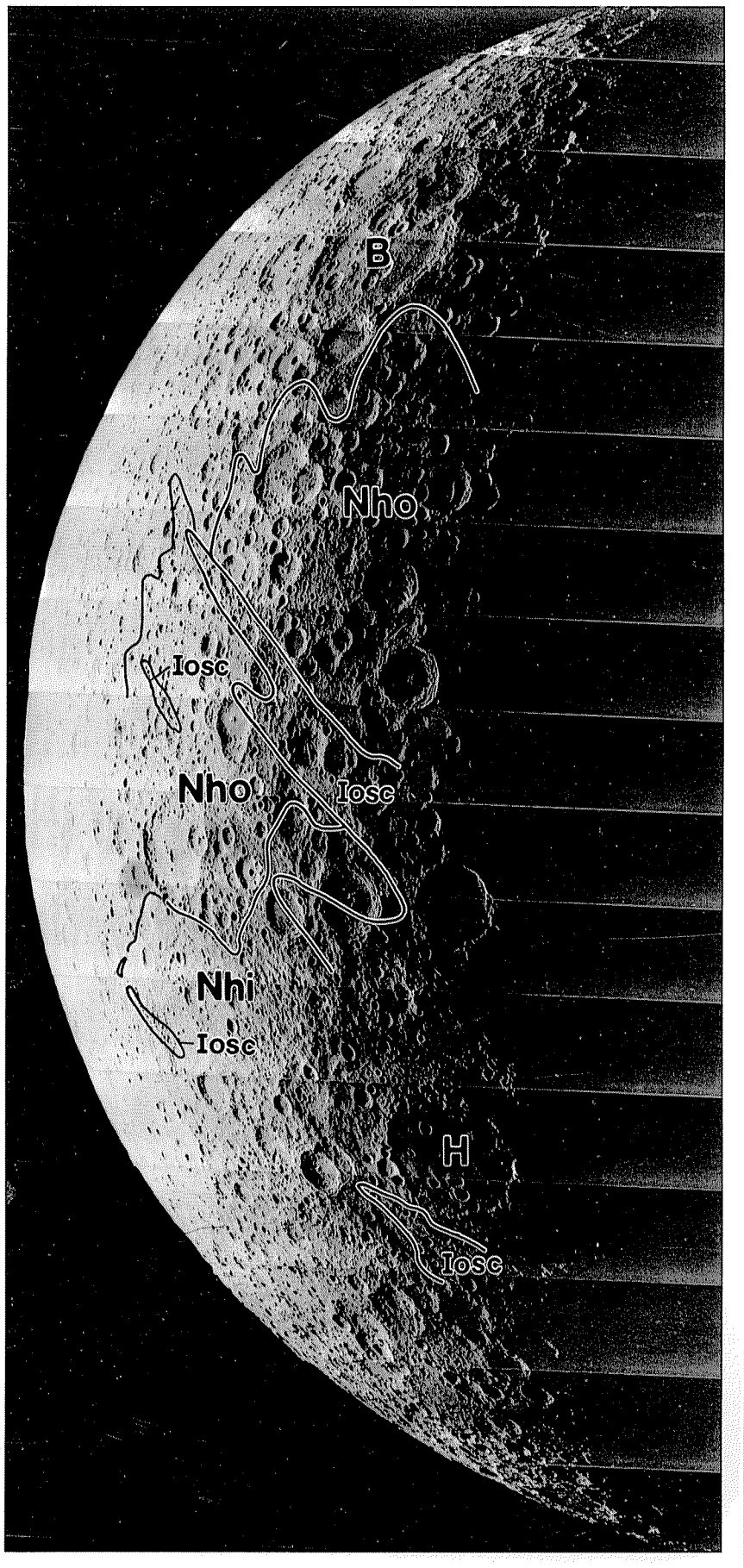

FIGURE 9.25.—Upper Nectarian Hertzsprung basin (H). Inner (Nhi) and outer (Nho) deposits are superposed on pre-Nectarian basin Birkhoff (B) and overlain by Orientale-basin secondaries (Iosc) (compare figs. 4.5, 8.14). Orbiter 5 frame M–28.

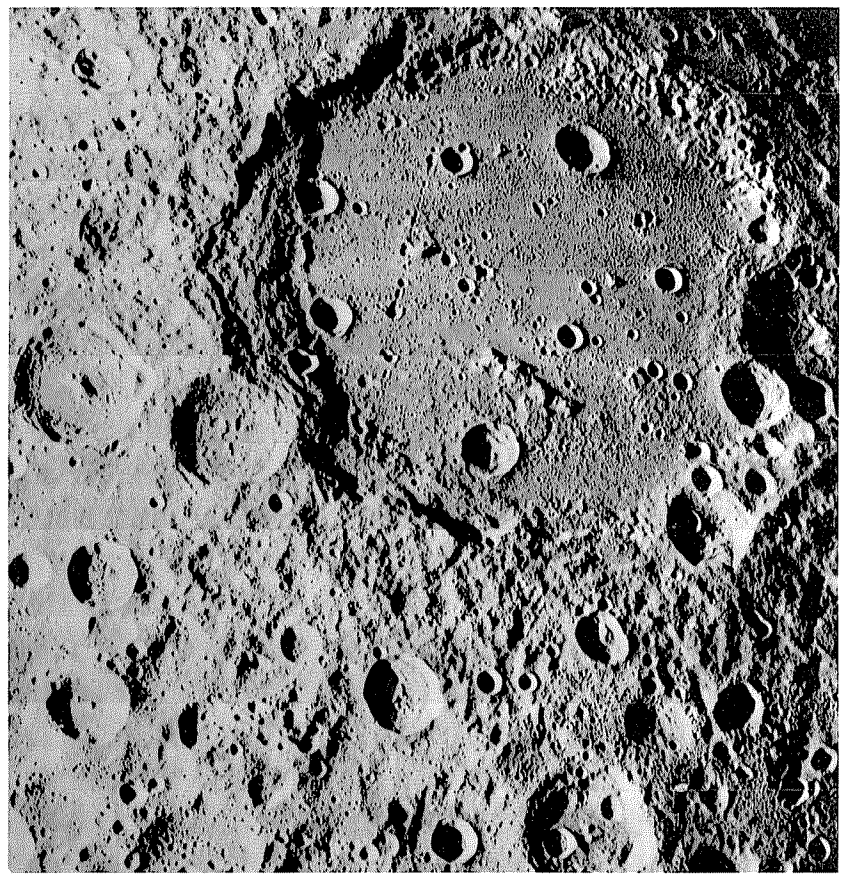

A

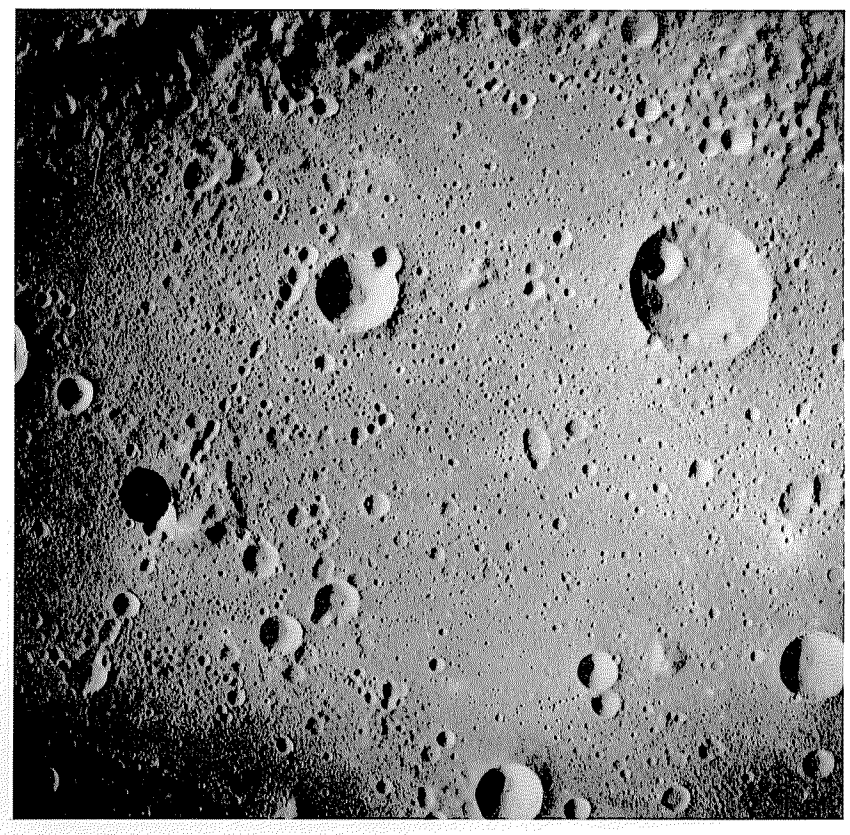

B

FIGURE 9.26.—Craterlike Nectarian basin Mendeleev, filled with Nectarian plains.

A. Part of radial ejecta and secondary field south of basin (between rim and lower edge of picture). Prebasin, mostly pre-Nectarian craters diminish in number and expression near rim. Orbiter 1 frame M–136.

B. Interior plains. Crater chain (Catena Mendeleev) is radial to, and undoubtedly secondary to, crater Tsiolkovskiy, 750 km south in direction of chain. Apollo 16 frame M–875.

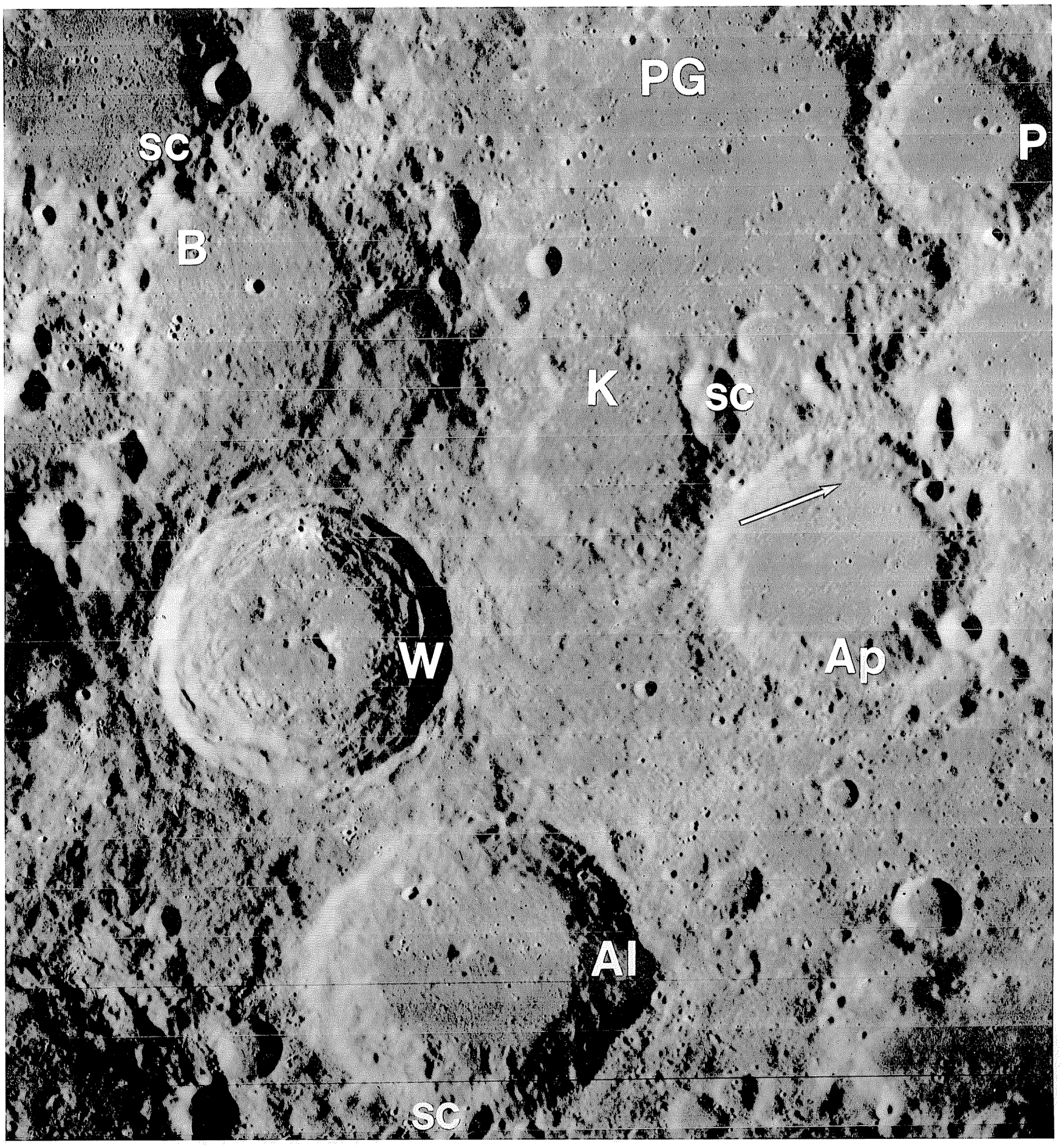

FIGURE 9.27.—South-central nearside (centered at 27° S., 5° E.). Apianus (Ap; 63 km) is lightly scored by lineations radial to Nectaris basin (Rupes Altai is 400 km in direction of arrow) and thus is probably pre-Nectarian. Playfair G (PG; 94 km), Krusenstern (K; 47 km), and Blanchinus (B; 61 km) are heavily mantled by probable Nectaris deposits and thus are pre-Nectarian; their rims are also nicked by Imbrium-basin secondaries (sc). Intercrater terrain probably consists mostly of Nectaris-basin deposits. Crater Aliacensis (Al; 80 km) would appear moderately fresh if it were not degraded by deposits of Werner (W; 70 km, Eratosthenian; compare fig. 3.26); Imbrium-basin secondary craters (sc) superposed on rim constrain age of Aliacensis to Nectarian. Playfair (P; 48 km) is also moderately fresh and probably Nectarian. Orbiter 4 frame H–101.

VOLCANIC ROCKS

Volcanism began on the Moon before the emplacement of the visible maria. This conclusion was reached even before any samples were examined, based on the reasoning that generation of basaltic magmas cannot have started coincidentally with the Orientale impact. Only post-Orientale maria can have remained exposed because all earlier maria were obscured by impacts (Hartmann and Wood, 1971; Shoemaker, 1972; Hartmann, 1973; Ryder and Taylor, 1976; Basaltic Volcanism Study Project, 1981, chap. 8). The high pre-Orientale impact rate must have kept lunar surfaces so thoroughly churned that extensive basalt flows did not long remain exposed, and Orientale and each earlier large basin impact must have covered most of the Moon with debris. Nor did the impacts trigger the volcanism; Orientale would be filled more deeply if it had triggered its own volcanic fill.

This well-founded inference is confirmed by physical evidence. Mare basalt has been found as fragments in bedrock breccia deposits (table 9.5; Ryder and Taylor, 1976; Ryder and Spudis, 1980). The Apollo 14 collection contains the most numerous of these samples, possibly because it contains material ejected from the already-flooded Procellarum and Insularum basins. This collection includes four large and several small samples of high-Al basalt, identified by cotectic compositions and the absence of siderophiles as endogenic, and by other chemical characteristics as related to mare basalt (Ridley, 1975; Taylor, 1975, p. 136; 1982, p. 300). Dated samples of high-Al basalt include the 251-g sample 14053 and 45-g sample 14072, found as individual rocks, and clasts from breccia sample 14321 (table 9.5). Additional high-Al basalt was found by Apollo 14 as small clasts in breccia samples (for example, fragments in sample 14063 with intermediate Ti contents; Ridley, 1975) and as fragments in the regolith (Ryder and Spudis, 1980). Apollo 17 fragment-laden impact-melt rocks also contain scattered small fragments of high-Al mare basalt (James and McGee, 1980). One sampled boulder contains clasts of basalt that may be intermediate between KREEP and mare basalt (sample 72275; Ryder and Spudis, 1980). The fact that relatively few samples of volcanic basalt have been discovered in terra breccia deposits is not surprising in view of the small volume of the crust composed of mare basalt today (see chap. 5). A major impact on any part of today's Moon would generate breccia much richer in terra material than in mare basalt.

The pre-Imbrian basalt fragments have been dated at from 3.85 to 3.99 aeons (combined range of ages obtained by Ar-Ar and Rb-Sr methods, table 9.5; Ryder and Spudis, 1980). If the Nectaris basin formed 3.92 aeons ago, these ages span the boundary between the Nectarian and pre-Nectarian; most are Nectarian.

TABLE 9.5.—*Absolute ages of some pre-Imbrian volcanic clasts*

[After Ryder and Spudis (1980).
Stations C2, C', and C1 are on rim flank of Cone Crater at the Apollo 14 landing site; 2(1), station 2, boulder 1, Apollo 17 landing site.
Ages are calculated using International Union of Geological Sciences (IUGS) radioactive decay constants (Steiger and Jäger, 1977), except the age determined by Husain and others (see headnote, table 9.1). Ar-Ar ages are ^{40}Ar-^{39}Ar plateau ages.
References: C72, Compston and others (1972); C75, Compston and others (1975); H72, Husain and others (1972); M73, Mark and others (1973); M75, Mark and others (1975); PW71, Papanastassiou and Wasserburg (1971b); S73, Stettler and others (1973); T71, Turner and others (1971; see also Turner, 1977); Y72, York and others (1972)]

Sample	Station	Lithology	Age	Method	Reference
14053	C2	251-g high-Al mare-type basalt.	3.88±0.04	Ar-Ar	S73
			3.88±0.04	Rb-Sr	PW71
			3.89±0.05	Ar-Ar	T71
			3.92±0.08	Ar-Ar	H72
14072	C'	45-g high-Al mare-type basalt.	3.91±0.09	Rb-Sr	C72
			3.91±0.14	Rb-Sr	M75
			3.93±0.12	Rb-Sr	M73
			3.98±0.05	Ar-Ar	Y72
Clasts in 14321	C1	High-Al mare-type basalt clasts (sample 14321 is diverse 9-kg breccia).	3.85±0.05	Ar-Ar	Y72
			3.87±0.04	Rb-Sr	PW71
			3.88±0.05	Ar-Ar	Y72
			3.93±0.05	Ar-Ar	Y72
			3.93±0.12	Rb-Sr	M73
			3.96±0.06	Rb-Sr	M73
			3.96±0.08	Rb-Sr	C72
Clasts in 72275	2(1)	Basalt intermediate between mare and KREEP types.	3.87±0.04	Rb-Sr	PW71
			3.93±0.04	Rb-Sr	C75

The extent of Nectarian and pre-Nectarian volcanism is unclear. If the heat source was entirely radiogenic (Taylor, 1982), the ancient basalt units were less extensive than the visible maria, because radioactive U, Th, and K are not abundant in the Moon. If, however, the Moon retained considerable primordial heat during its first aeon (Hubbard and Gast, 1971; Wood, 1972b; Toksöz and Johnston, 1974; Hubbard and Minear, 1975; Ryder and Taylor, 1976; Solomon and Head, 1979, 1980), only a small rise in temperature might have been sufficient to melt considerable magma.

Photogeologic evidence is consistent with considerable premare volcanism. Scattered patches of Nectarian plains have been identified in many parts of the terrae on the basis of crater densities (pl. 7; figs. 9.26*B*, 9.28, 9.29; Neukum and others, 1975b; Wilhelms and El-Baz, 1977; Stuart-Alexander, 1978; Lucchitta, 1978; Wilhelms and others, 1979). Some Nectarian plains, including the concentration in the Mutus-Vlacq basin already discussed (figs. 8.12, 9.2*B*), surround Nectarian basins and are stratigraphically related to the lineate deposits in the same way the circum-Orientale plains are related to the Hevelius Formation. That is, they are younger than the ejecta and secondary craters, but by an unknown amount. If they were part of the ejecta-deposition process, they are momentarily younger; if they are volcanic, they may be substantially younger.

Many of the plains may, in fact, have originated by a combination of volcanism and ejecta deposition. Eggleton and Marshall (1962) ascribed the planar light-colored surfaces south of the type area of the Fra Mauro Formation (figs. 10.18, 10.19) and elsewhere in the central lunar highlands to covering of premare surfaces by Imbrium ejecta. Wilhelms and El-Baz (1977) noted that the Nectarian and Imbrian plains in the Lomonosov-Fleming basin (fig. 9.28) are too smooth and extensive to be easily explained as basin ejecta and suggested that they were volcanically emplaced. Schultz and Spudis (1979) showed that the Lomonosov-Fleming plains are spotted by many dark-haloed craters that probably excavated dark material from beneath a lighter-colored cover. Therefore, the plains may consist of basaltic materials overlain by a thin cover of Crisium, Imbrium, or Orientale ejecta. Orientale ejecta may have covered basaltic plains in the Schiller-Zucchius basin near Orientale (Hartmann, 1966; Schultz and Spudis, 1979), which have diffuse patches darker than most terra plains (fig. 7.6; Offield, 1971). Numerous other plains, mostly inside basins of pre-Nectarian (Mutus-Vlacq) and Nectarian (Hertzsprung, Korolev) age, may also consist partly of premare basalt (pl. 7). Original emplacement in the style of the currently visible mare-basalt flows is indicated.

Geochemical sensing suggests that the dark halos contain both mare and KREEP basalt (Schultz and Spudis, 1979; Hawke and Spudis, 1980). Dark-haloed craters superposed on light-colored plains of Nectarian and Imbrian age (Wilhelms and El-Baz, 1977) within the possible Balmer-Kapteyn basin (table 4.2) display the telltale high radioactivity of KREEP (Haines and others, 1978), an observation suggesting impact exhumation of Nectarian or pre-Nectarian KREEP basalt (Hawke and Spudis, 1980). Mare basalt was probably exhumed from beneath the plains north of Taruntius and in many other localities (Schultz and Spudis, 1979; Hawke and Spudis, 1980). Therefore, basalt with a range of compositions may have been extruded far back into lunar history. The extent of this volcanism, however, remains uncertain.

CHRONOLOGY

If the age of 3.92 aeons favored here for the Nectaris basin is correct, then the Nectarian Period began 3.92 aeons ago and ended 3.85 aeons ago when the Imbrium basin was formed (see chap. 10).

One of the most frequently cited hypotheses in the lunar literature is that a "cataclysm" formed most or all basins within an interval of only 0.1 aeon (Tera and others, 1974). This cataclysm is generally conceived as a resumption of heavy bombardment after a lull following the heavy accretionary bombardment. The main basis for this hypothesis is that radiometric ages of terra rocks are concentrated around 3.8 to 3.9 aeons. Serenitatis looks like a relatively old basin; yet it has an absolute age that falls within this interval. The following data, presented here and in chapter 8, are consistent with the contrary view that the cratering rate declined relatively steadily (Baldwin, 1974b; Hartmann, 1975). (1) Numerous ages do predate 4.0 aeons (table 8.4; Baldwin, 1974b). (2) A concentration of late dates would be the natural consequence of a steadily declining cratering rate because of repeated impact reworking (Hartmann, 1973, 1975).

(3) No pre-Nectarian basins were sampled (fig. 9.30). (4) A smooth cratering curve (fig. 8.16) is fixed by a 3.92-aeon age for Nectaris, a 3.85-aeon age for Imbrium, and the ages of mare-basalt samples; this curve is consistent with a relatively young Nectarian relative age (table 9.3) and a 3.87-aeon absolute age for the Serenitatis basin. "Minicataclysms" forming some of the basin age groups are possible, but no cataclysm in the sense generally meant is recorded in lunar rocks. Instead, the record of early lunar impacts reveals a continuous barrage of large projectiles that only during the Nectarian Period began to approach less than cataclysmic proportions.

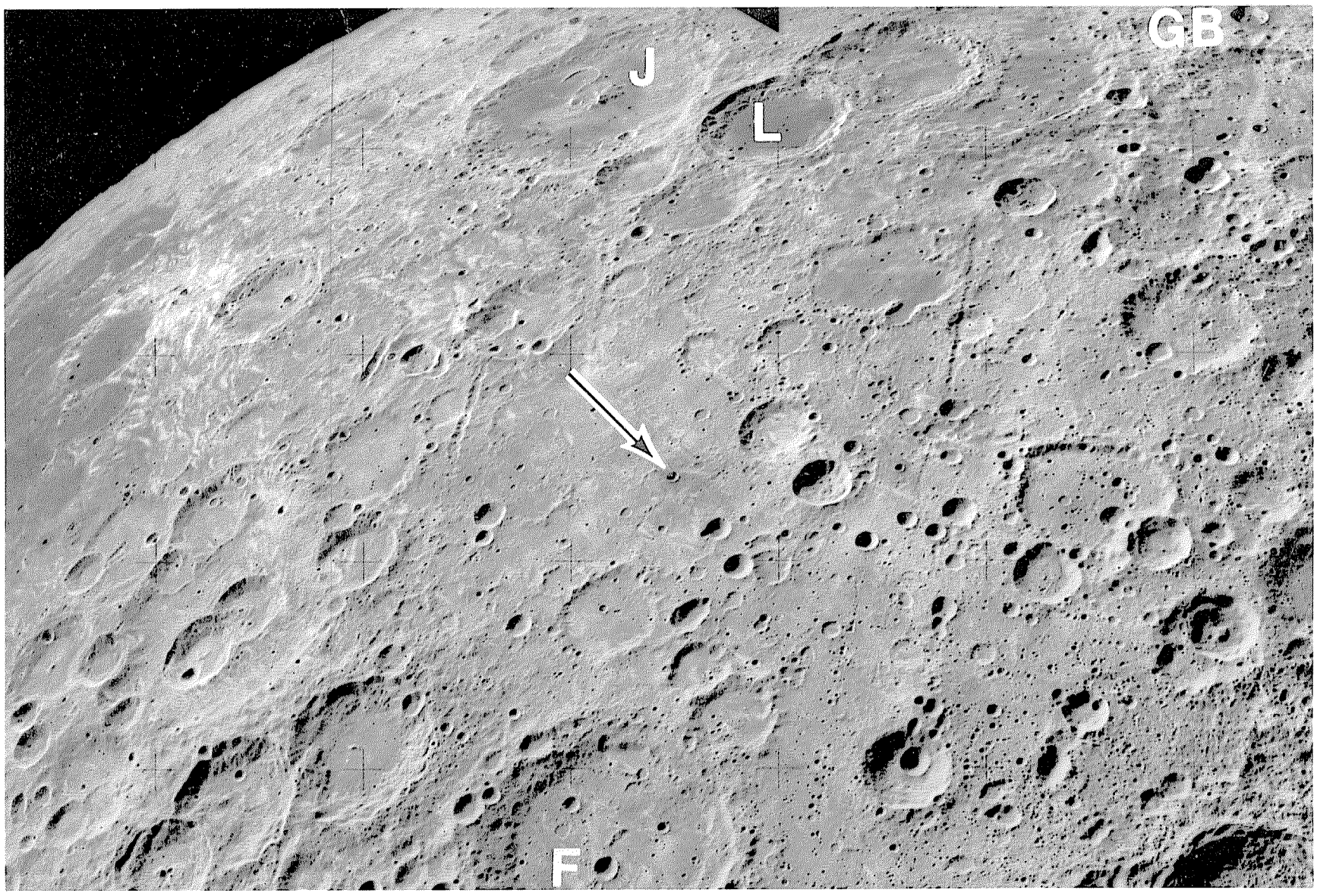

FIGURE 9.28.—Lomonosov-Fleming basin (compare fig. 8.13). F, Nectarian crater Fleming (130 km, 15° N., 110° E.). Dark halo (arrowhead) indicates basalt buried beneath light-colored Nectarian and Imbrian plains of probable basin origin. Mare fills crater Lomonosov (L; 93 km, 27° N., 98° E.), and Lomonosov ejecta is apparently covered by older mare in crater Joliot (under letter J); thus, Lomonosov is Lower Imbrian (compare fig. 4.7). Mare at left edge is Mare Marginis. GB, Giordano Bruno (22 km, 36° N., 103° E.), one of the Moon's youngest craters of its size. Apollo 16 frame M–3004.

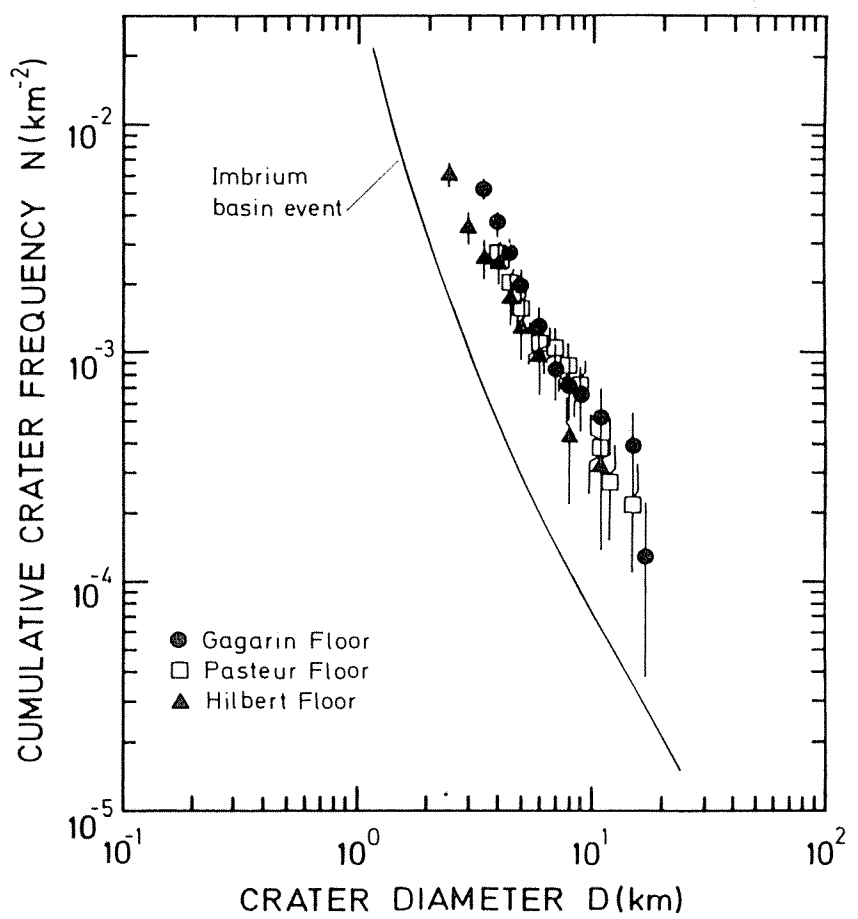

FIGURE 9.29.—Crater size-frequency curves by Neukum (1977), showing ages of plains in craters Gagarin, Pasteur, and Hilbert relative to Imbrium-basin deposits ("event"). Older, probably Nectarian frequencies are a factor of at least 7 higher than the Imbrium-basin frequency. Containing craters are pre-Nectarian (Gagarin and Pasteur) and Nectarian (Hilbert) (compare figs. 3.5, 8.11).

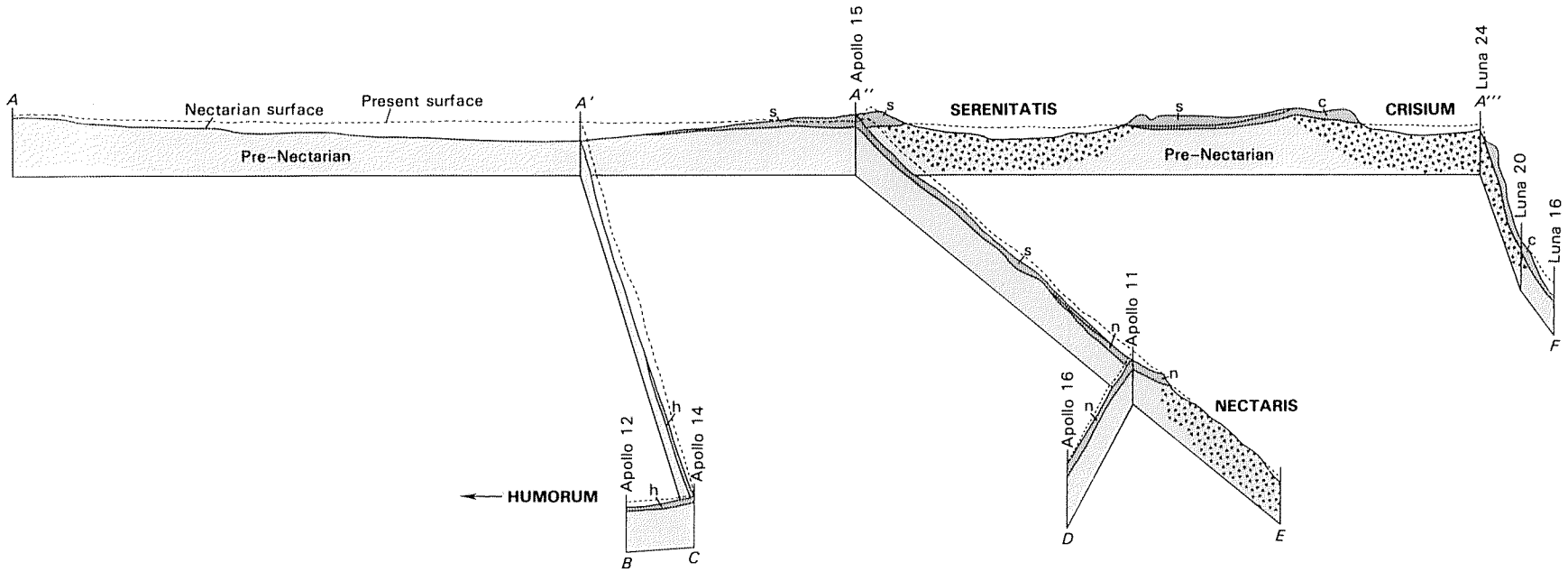

FIGURE 9.30.—Geologic cross sections based on figure 8.4*A*, showing deposits of the Nectarian basins Nectaris (n), Humorum (h), Crisium (c), and Serenitatis (s). Triangles, subbasin breccia (overlain by impact melt, not shown). Materials of the later Imbrium basin are derived partly from Serenitatis deposits and partly from pre-Nectarian terrane. Depression created by Procellarum basin (see fig. 8.4*B*) is still evident, though reduced by superposition of other pre-Nectarian deposits. Dotted lines, present surface.